Controlling oxygen sensors with an automotive microcontroller

DAMIEN CHAZAL

KTH Electrical Engineering

Masters' Degree Project
Stockholm, Sweden 2006

XR-EE-RT 2006:008

Abstract

Oxygen sensors are used in car engines to monitor the efficiency of the combustion process by measuring and adjusting the air/fuel mixture. There are two types of automotive oxygen sensors: lambda sensors which are only sensitive at the stoichiometric point and UEGO (Universal Exhaust Gas Oxygen) sensors that are able to detect a larger range of air/fuel ratios. UEGO sensors require a precise control of their temperature as well as the regulation of an internal electrochemical potential. These operations are usually realized by dedicated ASICs (Application-Specific Integrated Circuits) added to the engine ECU.

This thesis explores the possibility of controlling a UEGO sensor directly from the engine ECU. RENAULT has obtained a patent on this concept and this thesis aims to study its feasibility. The control system is based on a new generation of automotive micro controllers, the 32-bit Tricore familly from INFINEON, which will be used in future ECUs.

A description of how oxygen sensors work is first presented and is followed by an overview of the control strategy. The electronic interface between the sensor and the microcontroller comes down to a set of actuators and amplifiers. The two regulation tasks, which are totally handled by the micro controller, are based on many of its autonomous units in order to minimize the CPU-load. For each control loop, a model of the plant is derived to determine the best parameters of the PI controllers.

The sensor and its control system are finally tested on a gas bench under different air/fuel ratios. Conclusions about this control strategy are drawn.

Acknowledgements

Contents

List of symbols

Introduction

Oxygen sensors are one of the most critical sensors on a fuel-injected engine. They measure the amount of oxygen in the exhaust stream, allowing the engine ECU to control the efficiency of the combustion process in the engine. These sensors resemble a spark plug and are attached to the engine's exhaust manifold to determine whether the mixture of air and gasoline going into the cylinder is rich (too much fuel) or lean (too little fuel). This information is then sent to the engine management ECU computer, which adjusts the mixture to give the engine the best possible fuel economy and lowest possible exhaust emissions.

There are two types of ogygen sensors in automotive applications: lambda sensors and UEGO (Universal Exhaust Gas Oxygen) sensors. The voltage produced by lambda sensors is so nonlinear with respect to oxygen concentration that it is impractical for the ECU to measure intermediate values — it merely registers "lean" or "rich". New engines usually operate in the lean region to save fuel. It is thus impractical to control an engine in this range with a lambda sensor since it isn't sensitive in this area.

Contrary to lambda sensors, UEGO sensors deliver a proportional information about the air/fuel mixture. They are hence able to provide proper feedback for engines operating in the lean region. UEGO sensors are nonetheless much more complex than lambda sensors because they necessitate two regulation loops, one for temperature control and the other one for eletrochemical pumping control. The driving electronics are even more complex since the two feedback loops can interfere. RENAULT has hence investigated a way to reduce the cost of such devices by directly controlling the sensor by the engine ECU.

This thesis explores the possibility of controlling a UEGO sensor directly from an automotive microcontroller from the Tricore familly (INFINEON). First the sensor's behaviour is studied and modelled. Then the control strategy is built around the microcontroller with as little electronics as possible. Finally the performance of this control system is evaluated.

Chapter 1

Techniques for measurement of air-to-fuel ratio

High-temperature zirconia-based oxygen sensors are one of many types of oxygen sensors. They are particularly suited to the monitoring of AFRs in fuel combustion systems.

In this part the various techniques for measurement of oxygen concentration or partial pressure with sensors employing zirconia electrolytes are reviewed. Their application in AFR measurement is also discussed. Two types of sensors are used in automotive applications: Lambda sensors and UEGO sensors. This section aims to explain how these sensors work, from the most simple one (the Lambda sensor) to the most complex one (the UEGO sensor).

1.1 Principles of operation of electrochemical oxygen gas sensors

Electrochemical oxygen sensors employing zirconia electrolytes have gained popularity compared, for example, with aqueous electrochemical sensors for a number of reasons: the electrolyte in the former devices is non-volatile enabling operation in environments above ambient without solvent loss. Moreover, elevated temperature of operation can facilitate the catalysis of reactive gases such as CO_2 and CO, so that equilibrium gas concentrations may be measured in combustion processes. Finally, the response time to a change in gas concentration can be rapid (e.g $\approx$ 50 ms for a zirconia oxygen sensor in more than 1000 PPM O_2 at 700 °C).

1.1.1 The fundamental electrochemical cell

The collective term zirconia denotes a solid solution mixing ZrO_2 with aliovalent oxides such as CaO, MgO or Y_2O_3, referred to as stabilizers. In this mixing process, a small fraction of Zr^{4+} ions are replaced by lower valency ions such as Ca^{4+}, Mg^{2+} or Y^{3+} in order to create oxygen vacancies in the solid solution. As a result, oxygen ions can hop from one unoccupied site to the next. This mechanism is similar to the doping process in a p-type semiconductor, where a deficiency in electrons is obtained by adding ions into the structure.

The mobility of oxygen ions in zirconia is a thermally activated process becoming significant at temperatures above 300 °C. Therefore, when operated at high temperature, stabilized zirconia behaves as an electrolyte. The following picture (figure 1.1) represents a single electrochemical cell used for oxygen sensing or pumping. It includes two porous metal electrodes acting as an interface between the electrolyte and the external electronic

circuitry connected to it. The electrochemical reactions occur at the interface between the electrode, the electrolyte and the surrounding gas; this interface is referred to as the three-hase boundary. In Lambda and UEGO sensors, the electrolyte is made of Yttria Stabilized Zirconia[1] and Platine electrodes are used.
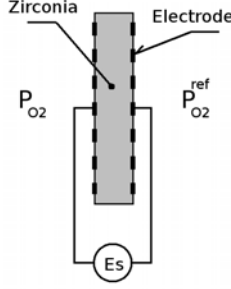
Figure 1.1: Schematic diagram of a single electrochemical cell.

The cell (1.1) develops an `EMF` generated by the tendency of oxygen ions within the electrolyte to drift from the high to low oxygen partial pressure side. When in contact with two atmospheres with oxygen partial pressure P_{O_2} and $P_{O_2}^{ref}$, the `EMF` is given by the Nernst equation[2]:

$$E_s = \frac{RT}{4F} \ln \left(\frac{P_{O_2}}{P_{O_2}^{ref}} \right) \tag{1.1}$$

If $P_{O_2}^{ref}$ is a known reference gas then P_{O_2} may be determined from a measurement of E_s at a given operating temperature. Thus the cell may be used as a *gauge* for the measurement of unknown oxygen partial pressures. This is the first operating mode of an electrochemical cell, also called *Nernst cell*.

It can also act as an electrochemical *oxygen pump* : by applying a current across the electrodes, oxygen may be electrochemically transferred from the cathodic to the anodic side of the cell. The electrode reaction is $O_2 + 4e \rightleftharpoons 2O^{2-}$: oxygen is reduced on the cathode and the resulting oxygen ions diffuse through the electrolyte to produce free oxygen at the anode side. The flux of oxygen transferred through the electrolyte is related to the applied current I_p by Faraday's law :

$$\frac{dn_{O_2}}{dt} = -\frac{I_p}{4F} \tag{1.2}$$

The negative sign is due to the oxygen flux being in the opposite direction to the pumping current. The factor of four is due to the fact that four electrons are involved in the pumping of one molecule of oxygen.

The following is a review of the two basic configurations for measurement of oxygen using zirconia sensors constructed around the fundamental cell described above: the *potentiometric* and the *amperometric* oxygen detection devices, which are respectively the basis structures of Lambda and UEGO sensors.

1.1.2 Potentiometric sensors

This type of sensor (also called lambda sensor) is based upon a single electrochemical cell (1.1) operated as a gauge (equation 1.1). The reference oxygen partial pressure is

---

[1] $(ZrO_2)_{0.92}(Y_2O_3)_{0.08}$

[2] Derived from the Boltzmann distribution $\frac{c_1}{c_2} = exp\left(-\frac{e\Delta U}{kT}\right)$, c_i denoting the concentrations of carriers in the two materials in contact

generally obtained from uncontaminated air, as shown on picture 1.2 and a heater is usually added close to the sensible element to operate at high temperature. Potentiometric sensors produce a logarithmic output based on the Nernst relation (1.1) and their use in combustion systems will be discussed further.
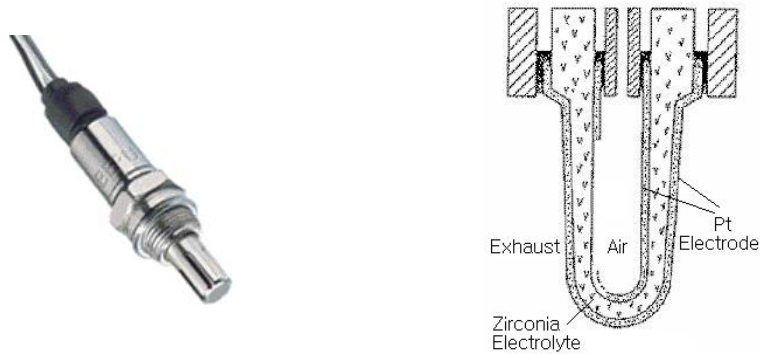
Figure 1.2: A lambda sensor

1.1.3 Amperometric sensors

Amperometric sensors are based upon the *pump* mode of operation of the electrochemical cell. The structure of such sensors is illustrated on Figure 1.3. An amperometric sensor is a combination of a pump cell and a gauge cell, enclosing an internal volume connected to the external atmosphere via a diffusion path usually made of a porous material.
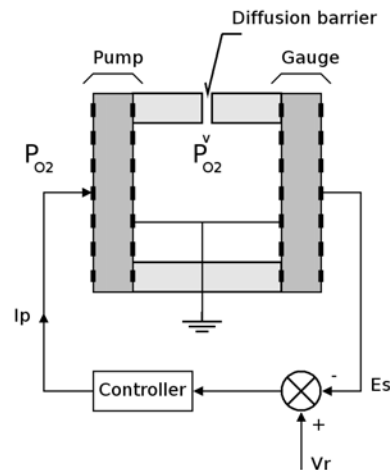
Figure 1.3: Operation of a singe-chamber oxygen pump-gauge with a constant gauge `EMF`.

The following analysis is given for a device operating in a gas mixture containing free oxygen and in steady state. The convention adopted is that a positive current pumps oxygen out of the internal volume.

By applying a positive current I_p to the pump, oxygen may be electrochemically removed from the internal volume. The flux of oxygen pumped out through the electrolyte is given by equation (1.2). Simultaneously, there will be oxygen leaking into the internal volume through the diffusion barrier. According to Fick's first law of diffusion[3], the flux

---

[3]Assumption : uniformity of the oxygen partial pressure within the diffusion hole

of oxygen leaking is given by $\sigma_{O_2}(P_{O_2} - P_{O_2}^v)$. In the steady state, the amount of oxygen is exactly balanced by the oxygen leaking into the internal volume, revealing :

$$\frac{I_p}{4F} = \sigma_{O2}(P_{O_2} - P_{O_2}^v) \tag{1.3}$$

In order to have a proportional relation between I_p and the measured oxygen partial pressure P_{O_2}, a gauge measures the Nernst `EMF` (see Equation 1.1) between the internal volume and the sample gas. It provides the following information about $P_{O_2}^v$:

$$E_s = \frac{RT}{4F}\ln\left(\frac{P_{O_2}}{P_{O2}^v}\right) \tag{1.4}$$

Moreover, as shown on Figure 1.3, the device is operated in a feedback loop in which the pumping current is automatically adjusted to hold the gauge `EMF` at some predetermined value V_r. The internal oxygen partial pressure is then given by:

$$P_{O_2}^v = P_{O_2}\exp\left(-\frac{4F}{RT}V_r\right) \tag{1.5}$$

Thus, combining equations 1.3 and 1.5 gives:

$$I_p = 4F\sigma_{O_2}\left[\left(1 - \exp\left(-\frac{4F}{RT}V_r\right)\right)\right]P_{O_2} \tag{1.6}$$

I_p is proportional to the oxygen concentration in the sample gas and to the leak conductance. The current-voltage characteristics (see Figure 1.4) shows different plateaus at given oxygen partial pressure when the gauge voltage is set to a high enough value[4].
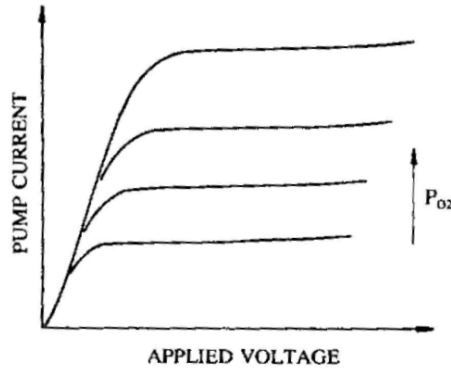
Figure 1.4: Current-voltage characteristics of an amperometric oxygen sensor at different oxygen concentrations

Contrary to potentiometric sensors, amperometric sensors deliver a linear response, provided that the Nernst voltage E_s of the gauge is regulated to a fixed value V_r typically around 500mV. Besides, amperometric sensors do not require a reference gas as long as they operate in gas mixtures containing free oxygen. However, some arrangements are necessary when these sensors are used for `AFR` measurement. Next part deals with this particular case and finally establishes the structure of UEGO sensors.

---

[4]$V_r \geq 50\text{mV}$ at $700\,^\circ\text{C}$ $\Rightarrow$ $I_p \approx 4F\sigma_{O_2}P_{O_2}$

1.2   Application to combustion processes

A major application of oxygen sensors concerns the determination of the AFR in combustion systems. The following is a discussion about the operation of the sensors described in the previous section with respect to AFR measurement.

1.2.1   Potentiometric sensors

The concentration of oxygen in the exhaust gases of a combustion system is related to the AFR by the complex chemical reactions occuring between the different gases in air with the fuel hydrocarbons (see Appendix A for more details). When air and gasoline are mixed together and ignited, the chemical reaction requires 14.7g of air to completely burn 1g of fuel. This air/fuel ratio is normalized to the Greek letter λ in such a way that when lambda equals 1, you have the stoichiometric ratio 14.7 : 1.

$$\lambda > 1 \text{ for a lean mixture}$$

$$\lambda < 1 \text{ for a rich mixture}$$

For typical conditions, the equilibrium partial pressure of oxygen varies with λ as depicted on Figure 1.5. Combining this with the logarithmic response of the potentiometric sensor, the overall sensor response changes over a very narrow lambda range. When the air/fuel ratio is perfectly balanced, the sensor produces a signal of about 0.45V. When the fuel mixture goes rich, the output shoots up quickly to 0.9V. Conversely, when the fuel mixture goes lean, the sensor's output drops to 0.1V. Lambda sensors are consequently
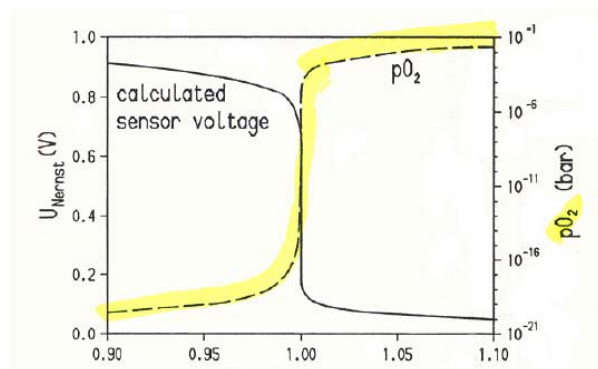
Figure 1.5: Output characteristic of a Lambda sensor measuring AFR

useful to detect the stoichiometric point ($\lambda = 1$) where the EMF shows a large change. However, in order to improve fuel economy, internal combustion engines are normally operated in the lean region ($\lambda > 1$) where the sensitivity of lambda sensors is low. This is the reason why linear oxygen sensors (based on the amperometric structure) are preferred in Diesel engines. Instead of switching back and forth from rich to lean, like Lambda sensor designs, these sensors produce a signal that is directly proportional to the AFR.

1.2.2   Amperometric sensors

The amperometric sensor considered previously can only be used where the AFR is lean of stoichiometry. This is a serious limitation and arises because potentials are essentially referred to that of the anode in the sample gas. In the lean region, the pump current I_p is proportional to the oxygen concentration and decreases towards zero as stoichiometry

is approached; in the rich region,due to the reduction of oxygen-containing species (e.g. CO_2, H_2O), the current rises again with the same sign as in the lean region. This problem of confusing the two sides of stoichiometry can be solved by immersing the anode of the amperometric sensor in an air reference at all times (see Figure 1.6).
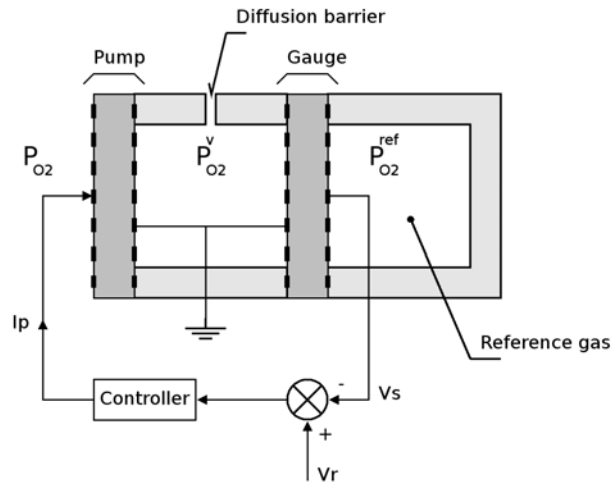
Figure 1.6: Amperometric sensor with reference gas operated with a constant gauge EMF

With only a small increase in complexity, the pump current shows reversal as stoichiometry is traversed and provides a measure of the AFR on both sides. The current-voltage characteristics of this sensor at different λ values is shown on Figure 1.7 as well as the $\lambda - I_p$ characteristics.
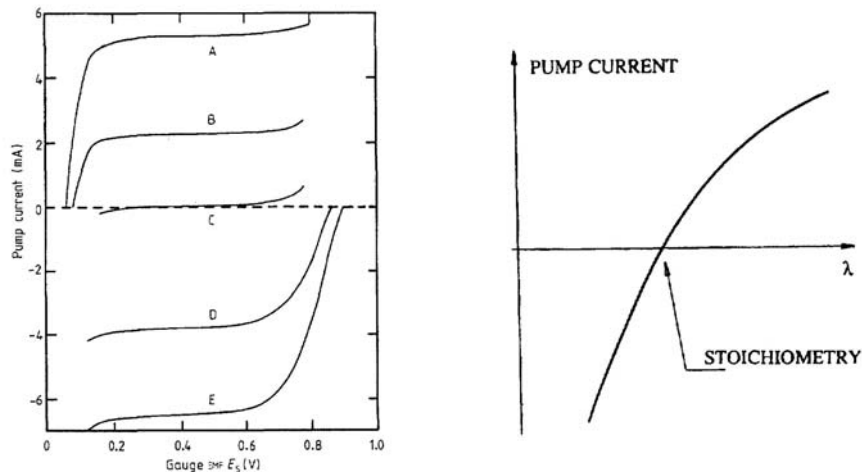
Figure 1.7: Sketch of the characteristics of sensors of UEGO sensors for various normalized AFR λ=(A,1.6; B,1.23; C,1.0; D,0.89; E,0.82). The stoichiometric point corresponds to $\lambda = 1$.

This final arrangement (see Figure 1.6) corresponds exactly to the structure of UEGO sensors, also called 'Wideband' oxygen sensors. The following section demonstrates theoretically how the application of a fixed gaseous reference to the gauge enables the regions $\lambda < 1$ and $\lambda > 1$ to be distinguished.

1.3   UEGO sensors

There many different UEGO sensors manufacturers but BOSCH sensors and control devices are the most widely used. In this section, two different UEGO sensors from BOSCH are considered: the `LSU4.2` and the latest one, the `LSU4.9` sensor.

1.3.1   Amperometric with stable reference (e.g. `BOSCH LSU4.2`)

The device of figure 1.6 distinguishes the two sides of stoichiometry thanks to the use of a reference gas of fixed composition like air. This can be demonstrated by determining the output of the sensor when operated in O_2-inert gas mixture (equivalent to the lean region) or $CO - CO_2$-inert gas mixture (equivalent to the rich region). The theoretical expressions for the output current I_p of the device in each case may be determined as follows.

Operation in lean region

As previously discussed (equation (1.3) to (1.6)) , the passage of the pump current I_p results in an oxygen flux through the electrolyte accompanied by a diffusive flux of oxygen through the leak. At steady state the sum of the two fluxes is equal to zero, revealing:

$$I_p = 4F\sigma_{O_2}(P_{O_2} - P_{O_2}^v)$$

The feedback loop adjusts $P_{O_2}^v$ aiming to maintain the Nernst `EMF` E_s constant and equal to V_r, but this time the gauge is in contact with the reference oxygen partial pressure $P_{O_2}^{ref}$, leading to:

$$V_r = \frac{RT}{4F}\ln\left(\frac{P_{O_2}^{ref}}{P_{O_2}^v}\right) \tag{1.7}$$

Eliminating $P_{O_2}^v$ between the two equations gives :

$$I_p = 4F\sigma_{O_2}\left[P_{O_2} - P_{O_2}^{ref}\exp\left(-\frac{4F}{RT}V_r\right)\right] \tag{1.8}$$

This equation predicts a linear variation of the current I_p with oxygen concentration[5] and $dI_p/dP_{O_2} > 0$.

Operation in rich region

The pump current I_p aims to adjust $P_{O_2}^v$ in order to maintain the gauge `EMF` equal to V_r (equation 1.7). For practical values for V_r (around 0.45V), this comes down to pump oxygen into the internal volume of the device since the reference gas (usually air) contains excess oxygen compared to the sample gas. However, as rich exhaust gases do not contain free oxygen, it cannot be pumped in directly but results from intermediate reactions.

The exhaust of internal combustion engines contains a variety of reactive hydrocarbons among which CO and H_2 are the most abundant species. It has been proved that CO — rather than H_2 — has the principal influence on the cell `EMF`. On the external electrode, the pump current I_p results mainly in reduction of CO_2:

$$CO_2 + 2e \rightleftharpoons CO + O^{2-}$$
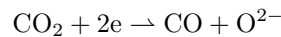
On the internal electrode, part of the current results in anodic oxidation of the CO present in the volume via:

$$CO + O^{2-} \rightleftharpoons CO_2 + 2e \tag{1.9}$$

---

[5]V_r is usually fixed to a high enough value, typically 0.45V, such that $\exp\left(-4FV_r/RT\right) \ll 1$, revealing a current I_p directly proportional to the oxygen partial pressure P_{O_2} : $I_p = 4F\sigma_{O_2}P_{O_2}$.

and the remainder generates free oxygen

$$2O^{2-} \rightharpoonup O_2 + 4e \tag{1.10}$$

Thus, the current I_p may be written $I_p = I_p^{CO_2} + I_p^{O_2}$, where $I_p^{CO_2}$ and $I_p^{O_2}$ are appropriate to equations (1.9) and (1.10). At steady state, for a given gas, the flux caused by the pumping current is counter balanced by the leak, which leads to the following equations:

$$
\begin{aligned}
I_p^{O_2}/4F &= \sigma_{O_2}\left(P_{O_2} - P_{O_2}^v\right) \\
I_p^{CO_2}/2F &= \sigma_{CO_2}\left(P_{CO_2} - P_{CO_2}^v\right) \\
&= \sigma_{CO}\left(P_{CO}^v - P_{CO}\right)
\end{aligned}
$$

where $P_{O_2} \approx 0$ and $P_{CO}^v \approx 0$ because the sample gas contains no oxygen and all the CO present in the internal volume has been oxidized by the current (equation (1.9)). The expression of I_p can be simplified to:

$$I_p = -2F\sigma_{CO}P_{CO} - 4F\sigma_{O_2}P_{O_2}^v$$

And finally, according to the gauge `EMF` (equation 1.7),

$$I_p = -2F\sigma_{CO}P_{CO} - 4F\sigma_{O_2}P_{O_2}^{ref}\exp\left(\frac{-4F}{RT}V_r\right) \tag{1.11}$$

This is the general expression for I_p in rich gas mixtures. It predicts the linear variation of I_p with the concentration of CO. Besides, the negative slope $\mathrm{d}I_p/\mathrm{d}P_{CO} < 0$ indicates that the sensor should enable the two sides of stoichiometry to be distinguished.

1.3.2   Amperometric with pseudo reference (e.g. `BOSCH LSU4.9`)

In the previous configuration, the provision of a fixed reference gas implies the use of a large enough reference chamber to counter act the natural diffusion of oxygen ions from the excess reference side to the pump side. The last generation devices tend to reduce the size of the sensible element, and hence the size of the reference chamber. The main drawback then lies on the difficulty to maintain a fixed composition reference gas.
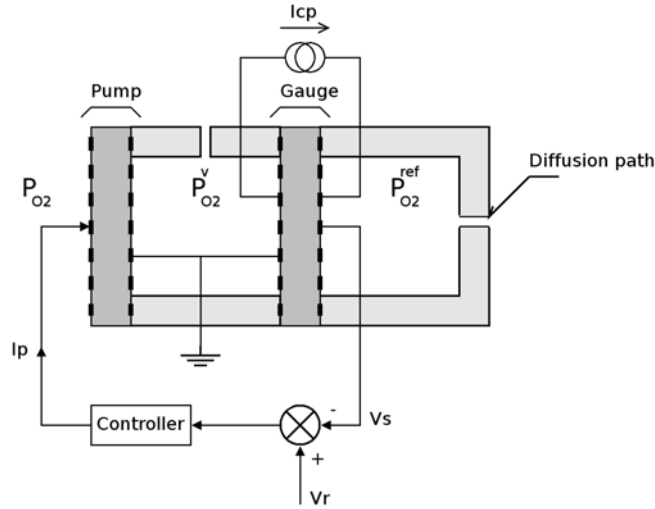
Figure 1.8: Schematic diagram of an amperometric sensor with pseudo-reference gas chamber.

The device of figure 1.8 contains a pseudo-reference chamber which is continuously regenerated in oxygen thanks to a constant pumping current I_{cp} that electrochemically pumps oxygen into the chamber. This oxygen is obtained from the reduction of oxygen-containing species in the sample gas. In this case, the precise composition of the reference gas is not critical provided that it is maintained with excess oxygen. A diffusion path is also added to balance the pressures on both sides of the pseudo-reference chamber. Sensors based upon this principle enable the two sides of stoichiometry to be distinguished without the need for a stable reference gas. The following is an analysis of the output current in the lean and rich regions.

Operation in lean region

As explained previously, the steady state equilibrium at the pump chamber between the amount of oxygen pumped out by the currents I_p and I_{cp} and the diffusive flux of oxygen through the leak reveals:

$$I_p = -I_{cp} + 4F\sigma_{O_2}(P_{O_2} - P_{O_2}^v) \tag{1.12}$$

The same equilibrium is reached at the reference chamber, yielding:

$$P_{O_2}^{ref} = I_{cp}/4F\sigma_{O_2}^{ref} + P_{O_2} \tag{1.13}$$

where $\sigma_{O_2}^{ref}$ denotes the leak conductance of the reference diffusion path. Considering the gauge EMF, expressed at equation (1.7) and eliminating $P_{O_2}^v$ inside equation (1.12), the steady state pump current becomes:

$$I_p = 4F\sigma_{O_2}\left[1 - \exp\left(-\frac{4F}{RT}V_r\right)\right]P_{O_2} - \left[1 + \frac{\sigma_{O_2}}{\sigma_{O_2}^{ref}}\exp\left(-\frac{4F}{RT}V_r\right)\right]I_{cp} \tag{1.14}$$

The output current I_p varies linearly with the oxygen concentration and $dI_p/dP_{O_2} > 0$.

Operation in rich region

The same analysis as for the stable reference sensor can be derived and would lead to the same conclusions about the ability of the sensor to distinguish the two sides of stoichiometry. The computations become too complex in this case but they are all based on the same discussions.

Chapter 2

Structure of the control system

In this chapter the structure of the UEGO control system is discussed. It consists of an automotive micro controller which drives the whole device and of an electrical circuit which acts as an interface between the sensor and the I/O of the micro controller. In this control system, two variables have to be under control: the internal temperature T which must be stabilised at 780 °C and the the Nernst `EMF` E_s which must be driven to a high enough value (typically 0.45V). The corresponding pump current I_p carries the information about the `AFR` and must be converted considering a nominal $I_p - \lambda$ characteristic. The control tasks are exclusively handled by the microcontroller which implies that the electronic part must be reduced to data acquisition and signal generation tasks.

2.1 General principle

Following is a brief description of the global system that can be summarized like in diagram 2.1. It comprises three parts: the sensor and its six connection points, a hardware electronic stage and a software stage based on the microcontroller.

2.1.1 Description of the `LSU4.X` UEGO devices

During this project, most of the experimentations have concerned the `BOSCH LSU4.9` sensor which is the most recent UEGO sensor available. The `BOSCH LSU4.2` sensor mainly differs from the way that the reference chamber is constructed but the specifications of the two sensors remain very similar. Therefore, most of the following descriptions apply to both sensors, except if mentionned.

A part from their connectors, UEGO sensors look very similar to conventional Lambda sensors. The exhaust gases enter in contact with the sensing element by circulating inside the sensor's head as shown on Picture 2.3. The pumping and sensing cells as well as the pump and the reference chambers coexist in a package that contains the heater element. A cross section of the sensing elements of the `LSU4.2` and the `LSU4.9` is represented in Appendix B.1.

A `BOSCH` UEGO sensor is a 6-wire sensor connected as shown on Figure 2.1. Below is a brief description of the different constitutive elements:

The heater (Pins 3-4)

The sensor is maintained at 780 °C thanks to the dissipation of a regulated power through a heating resistance of approximately 3.2Ω. The heating power is modified by PWM modulation of the continous $V_{\text{batt}} = 12$V power supply at a frequency of 100 Hz. When the heater is switched on, its power must be limited to avoid thermal stresses (refer to

15
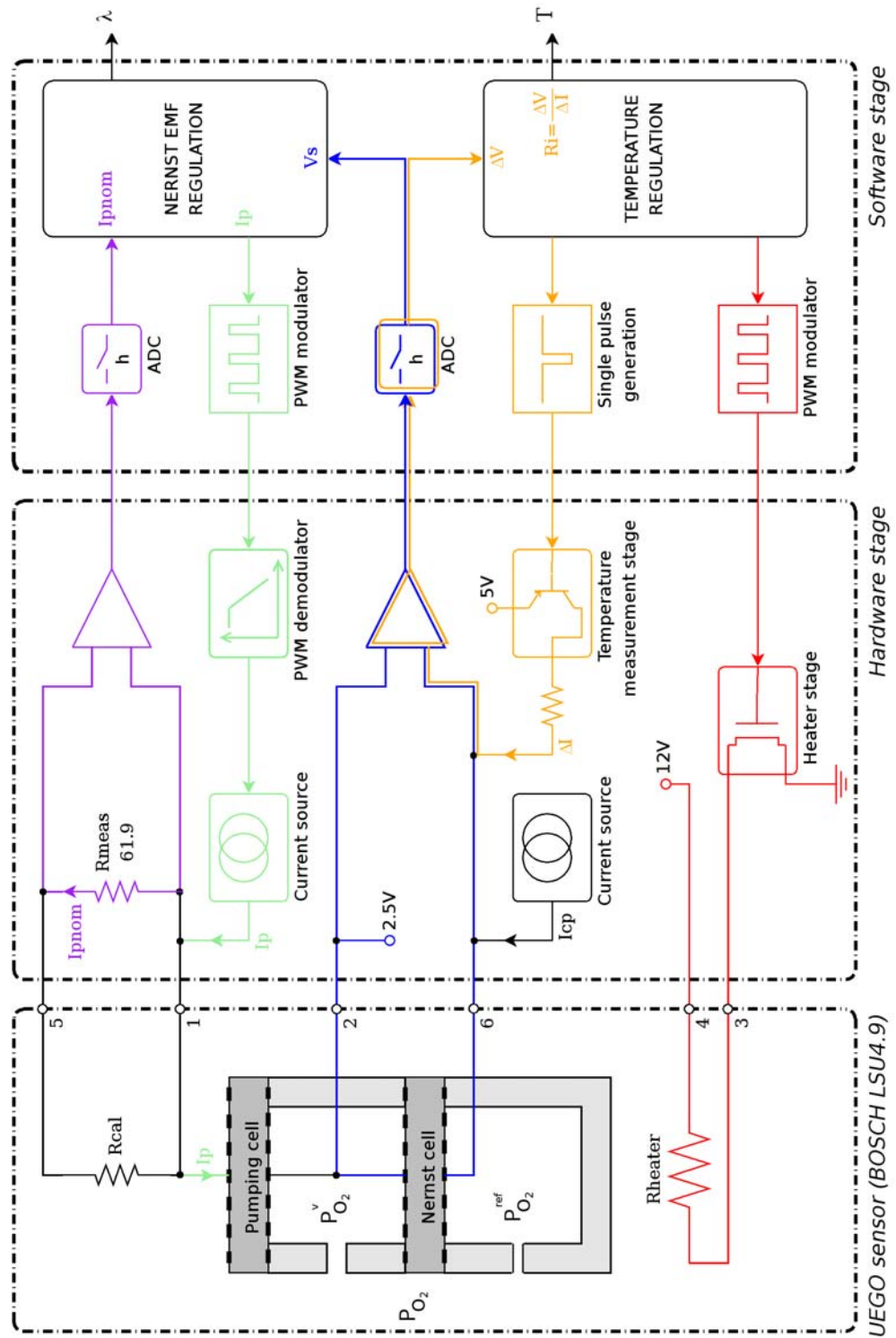
Figure 2.1: Overview of the control system: internal temperature measurement (orange), heater (red), Nernst voltage measurement (blue), pump current generation (green) and nominal current measurement (purple)

Figure 2.2: Picture of a `BOSCH LSU4.X` sensor.

Figure 2.3: Protection cover of `LSU4.X` sensors

Figure 2.4). First, the initial value of the effective heater voltage[1] V_H^{eff} is set according to the temperature of the device at start. Besides, the heat-up phase must be limited to a ramp rate $\Delta V_H^{\text{eff}}/\Delta \text{t} < 0.4\text{V/s}$ until the full power is reached ($V_H^{\text{eff}} = V_{\text{batt}}$). The sensor temperature can then be regulated to its final value.

Nernst cell electrodes (Pins 2-6)

The Nernst cell `EMF` can be measured between pins 2 and 6. The maximum current load that can be applied to a $\lambda = 1$ Nernst cell is $250\mu\text{A}$. In the case of the `LSU4.9` sensor, a constant reference pump current I_{cp} must be applied at the reference electrode (pin 6) in order to maintain excess oxygen in the reference chamber. The recommended value to be employed is $20\mu\text{A}$.

Pump cell electrodes (Pins 1-2)

The pump cell is connected between pin 1 and 2. The current going through this cell can be positive and negative depending on the `AFR`. Consequently, the internal electrodes of the pump cell are both connected to a virtual positive ground of 2.5V. This allows the generation of a negative pump current by applying a positive voltage below 2.5V at Pin 1.

The pump current must not exceed 6mA for lean gases and -9mA for rich compositions. Furthermore, no electrochemical pumping must be done before the sensor temperature reaches $600\,^{\circ}\text{C}$, otherwise there is a risk of blackening[2].

---

[1]duty cycle $= \left(V_H^{\text{eff}}/V_{batt}\right)^2$

[2]this phenomenon actually occurs when three conditions are met at the pump cell: ($T < 600\,^{\circ}\text{C}$, $\lambda > 1.25$ and $V_p > 1.8\text{V}$), V_p denoting the pump cell `EMF`

$T_{\texttt{Sensor}}$ / °C		-40	-10	20	50
$V_{\texttt{H,eff,max}}$ (t=0) /V		8.5	9.5	10.5	10.5
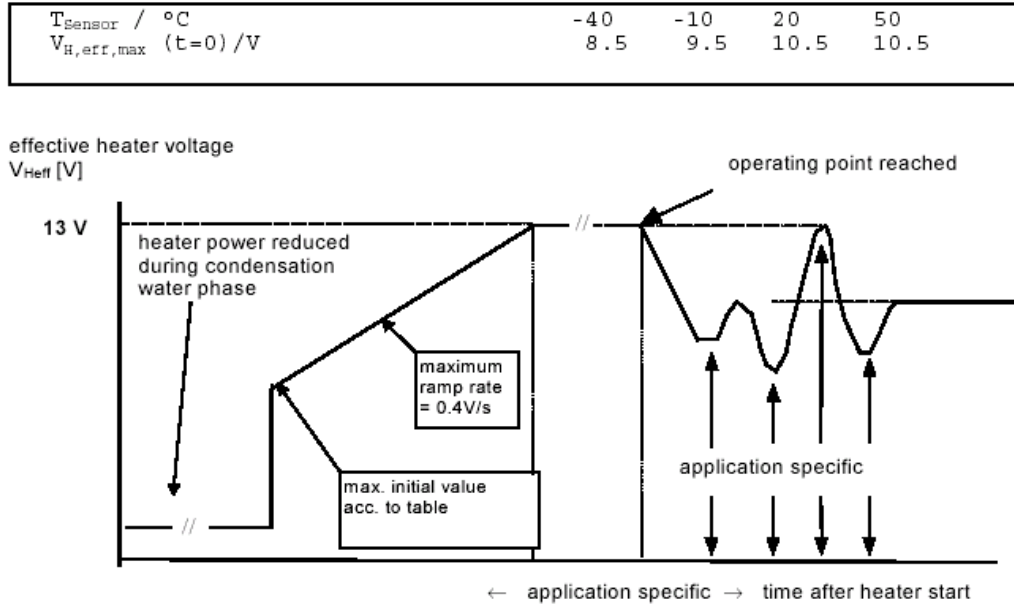
Figure 2.4: Maximal permissible heat up rate with limited heater power to reduce the thermal stresses in the heat-up phase

Calibration resistance (Pins 1-5)

All sensors have to deliver the same $I_p - \lambda$ characteristic to avoid a calibration procedure each time a UEGO sensor is implemented on a vehicle. For this purpose, BOSCH has equipped every sensor with a calibration resistance R_{cal} located inside the connector. When it is coupled with a measuring resistance R_{meas} of 61.9Ω, the proportion of current going through R_{meas} corresponds to the nominal output current.

The calibration procedure consists in modifying the value of R_{cal} via a laser operation while the sensor is operating in a predetermined gaseous composition until the sensor delivers the same output characteristics as the nominal one shown in Appendix B.5. More details about this nominal output current are given in Appendix B.2.

2.1.2   Control mechanism

Before going further into details, let us describe how the software together with the hardware stage are designed to drive the sensor at its operating point.

Nernst EMF and pump current measurement

The Nernst potential V_s denotes the voltage drop at the sensor's outputs between pin 2 and 6. It is identical to the Nernst EMF E_s when no current is running through the Nernst cell. The reason is that when operated at 780 °C, the Nernst cell is equivalent — as a first order approximation — to a Thevenin voltage source E_s associated with an internal resistance R_i. E_s typically ranges from 50mV to 0.9V like the output voltage of a lambda sensor. This signal is consequently amplified before being sampled by an ADC unit of the micro controller (see the blue circuit on Figure 2.1). One will note that V_s is measured in relation to the virtual ground potential of 2.5V.

The nominal pump current $I_{p_{nom}}$ is measured between pin 1 and 5. The corresponding voltage drop across $R_{meas} = 61.9\Omega$ is either positive or negative and does not exceed 100mV according to the pump current typical values. It must hence be amplified and also

shifted up to a positive range to fit the ADC conversion levels (0-3.3V or 0-5V depending on the type of micro controller). Only then can the normalized AFR be computed by looking up to the $I_p - \lambda$ characteristic.

Temperature measurement

As it was said previously, the Nernst cell is equivalent to a Thevenin voltage source E_s associated with an internal resistance R_i. The value of this resistance varies with respect to the temperature according to a relation $R_i = f(T)$ represented in Appendix B.3. The reference regulation temperature $T_{ref} = 780\,°C$ corresponds to an internal resistance R_i approximately equal to 300Ω for the `LSU4.9` UEGO sensor (80Ω for the `LSU4.2`). For temperatures varying between $650\,°C$ and $1200\,°C$, R_i ranges from 900Ω to 60Ω. It is hence possible to obtain a good estimation of the internal temperature T by measuring the internal resistance of the Nernst cell.
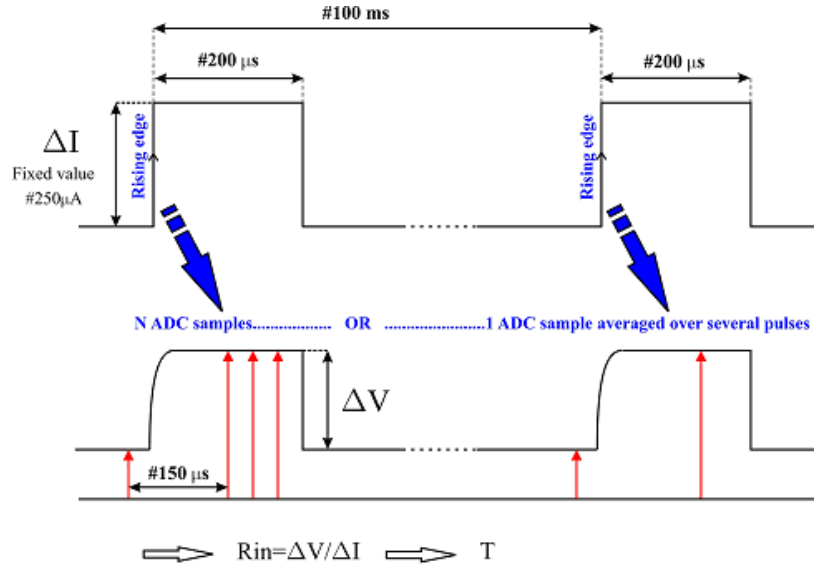
Figure 2.5: How the Nernst cell internal resistance is measured

R_i can be measured by applying a current pulse ΔI to the sensor and measuring the corresponding voltage pulse ΔV. The internal resistance is then determined by the ratio $\frac{\Delta V}{\Delta I}$ (see Figure 2.5).The length ($200\mu s$) and the frequency (10Hz) of this pulse are limited in such a way that the sensor is not electrochemically disturbed. A capacitive phenomena actually occurs if the measurement waveform longs too much.

The temperature measurement circuit appears in orange on Figure 2.1. A part of it overlaps the Nernst voltage measurement circuit (in blue), meaning that the Nernst voltage loop and the Temperature regulation loop can interfere. The voltage jumps due to R_i measurements can indeed disturb the Nersnt `EMF` regulation and result in a periodic pump current overshoot.

Three solutions are then conceivable:

- First, the use of a very high sampling frequency (much faster than the pump-gauge dynamics) for the temperature regulation coupled with an appropriate low pass filter can reduce the interferences between the two systems. Basically, a 3kHz signal is often used in some control devices to estimate the internal resistance. The main drawback of such a method is that it seems inadequate regarding the typical response time of the sensor temperature loop which is about a couple of seconds.

- Another realization consists in freezing the Nernst `EMF` control loop as soon as a current pulse is sent to the Nernst cell for temperature estimation. This solution is implemented on some electronic control devices incoporating an electrical switch that periodically opens the regulation loop.

- The last solution is derived from the previous one but does not require any additional electronic component to separate the loops. It simply consists in isolating by software the acquisitions related to temperature estimation from the regular ones intended for Nersnt `EMF` control. Each time a R_i measurement is required, a single pulse is generated and triggers two samples of V_s (one before the pulse and one at the end of the pulse) which are exclusively used to compute the value of R_i. This solution implies the use of a micro controller in order to clearly distinguish the different samples.

This last method is obviously the one that has been chosen for this project since it simplifies the electronics and turns out to be the less intrusive way to measure the temperature with respect to the Nernst `EMF` control loop.

Pump current generation

The pump current that must be applied to the pump cell is pulse-width-modulated by the micro controller like the heater command . The choice of the modulation frequency is discussed in the following section, as well as the demodulation circuit. In a few words, it comprises a low pass filter and a current source that converts the demodulated voltage to a positive or negative pump current.
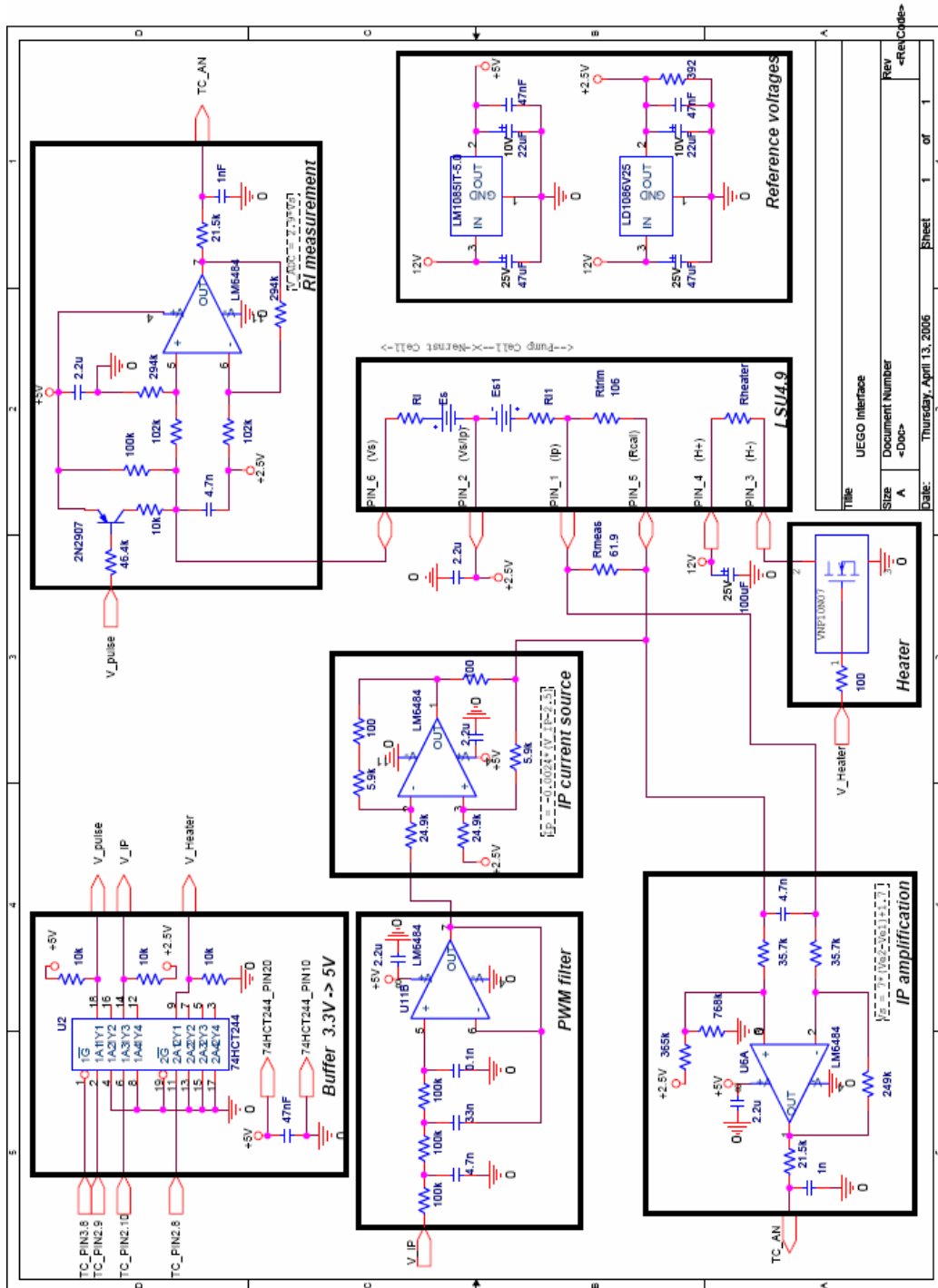
Figure 2.6: Electronic control circuit

2.2 Electronic interface

This section describes how each function of the hardware electronic stage (see Figure 2.1) is designed. The whole circuit linking the sensor to the micro controller is represented on Figure 2.6. A condensed version corresponding to the physical layout is attached in Appendix C.2.

2.2.1 General features

Following is a picture of the global system including the electrical circuit inserted between the microcontroller and the oxygen sensor (see Figure 2.7).
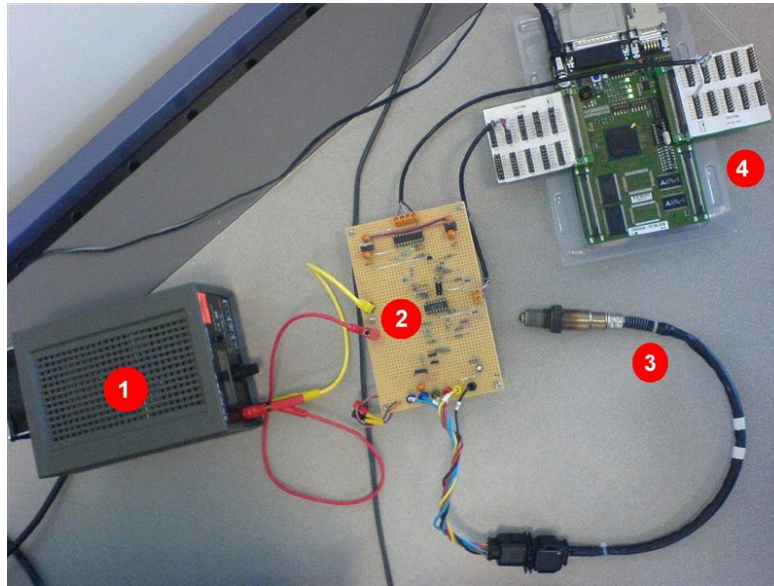
Figure 2.7: A picture of the global system (1: 12V power supply; 2: Electronic interface; 3: UEGO sensor; 4: Microcontroller mounted on its development board)

Reference voltages

Three fixed reference voltages are required in this design: 12V for the heater, 5V and 2.5V for the Nernst and pump cells electronics. A single 12V-voltage source is used and the other references are derived from it with the help of two voltage regulators (the `LM1085IT-5.0` and the `LD1086V25` respectively for the 5V and 2.5V reference voltages).

One will note that the 2.5V-regulator's output is connected to ground via a 392Ω resistor, creating a constant +6mA current flow out of the regulator. Such a trick enables the 2.5V virtual ground to absorb negative currents up to 6mA while keeping a positive current balance at the regulator. This correction has turned out to be essential probably due to the use of a non-symmetric regulator.

Output buffer

Depending on the micro controller technology being used, the digital output level is either 5V or 3.3V. The electronic circuit is conveniently based on a 5V level, which implies a systematic conversion of the output signals when employing 3.3V-micro controllers. Such an operation is realized by an octal 3.3V→5V buffer, the `74HCT244` microchip. The three outputs of the micro controller corresponding to the PWM command, the PWM pump

current command and the R_i measurement pulse are converted from 3.3V to 5V by the buffer.

An additional digital output is provided in order to enable or disable the buffer which is a 3-state device, meaning that when it is disabled, it has floating outputs. It is then possible to force the output states with pull-up or pull-down resistors when the micro controller is not connected for example. This feature is very important since it avoids driving the sensor in dangerous states (like low temperature and non-zero pump current). In practice, when the micro controller is not running, the heater command is pulled down to ground, the pump current command is driven in the 2.5V state and the R_i measurement output is pulled-up to 5V.

Heater stage

The heating circuit must be as much as possible isolated from the rest of the electronics because it employs high currents which can cause disturbances. It must consequently be connected close to the 12V-voltage source via separate wires. The `VNP10N07` is a power MOSFET enabling a current limitation of 10A for safety reasons. It behaves like a switch connecting and disconnecting the 12V-power supply to the heating resistor depending on the heating PWM command.

2.2.2 Nernst cell electronics

The electrical circuit connected to the Nernst cell (Figure 2.8) is in charge of three functions: amplification and scaling of the Nernst Voltage V_s; application of a single pulse for temperature estimation; generation of a constant reference pump current I_{cp}. All these functions are detailed below.
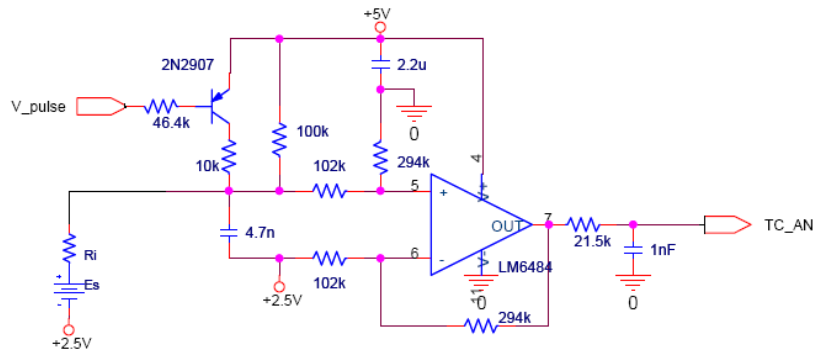
	min	max	typical
V_s	0V	0.8V	0.45V
V_{ADC}	0V	3.3V	1.3V
Operating ratings			
R_i	0Ω	2kΩ	300Ω
E_s	0V	0.8V	0.45V

Figure 2.8: Nernst cell electronic stage

Single pulse generation

In order to measure its internal resistance R_i, a short current pulse is applied to the Nernst cell. The current source is actually realized by a thevenin voltage source 5V/10kΩ

connected to pin 6 and commanded by a PNP bipolar transistor operated like a switch. The micro controller outputs a 0V-pulse that saturates the transistor during 200μs and the induced current flowing through the cell is approximately equal to 250μA under typical conditions[3].

V_s amplification

The Nernst voltage V_s is measured referring to the 2.5V virtual ground. A difference amplifier is used to precisely amplify the difference between the floating V_s and the 2.5V virtual ground. The gain of the amplifier is determined by the resistance ratio 294kΩ/102kΩ ≈ 2.9 so that the output voltage (referring to ground) does not exceed 3.3V, especially when a voltage pulse is applied to the Nernst cell. The input-output characteristic is:

$$V_{ADC} = 2.9 V_s$$

There is a risk of saturation at the ADC when R_i and E_s exceed certain values. The situation is particularly critical during the heat-up phase, when R_i is high and in presence of a rich mixture ($E_s \approx 0.8V$[4]). In this case, the voltage drop accross R_i during a temperature measurement added to E_s may lead to an output voltage higher than the 3.3V of the ADC. Table 2.8 sums up all these operating conditions. Figure 2.9 shows the amplified signal for different R_i and E_s when a measurement pulse is applied to the sensor.
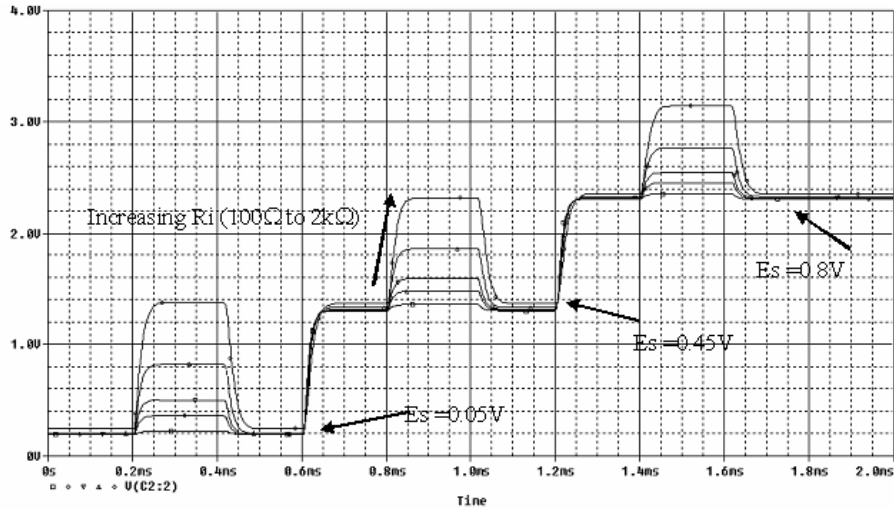
Figure 2.9: Output signal for different R_i [100Ω-2kΩ] and E_s {0.05V,0.45V,0.8V}

I_{cp} generation

The constant reference pump current I_{cp} results from a thevenin voltage source 5V/100kΩ applied to pin 6 of the sensor. Under operating conditions[5], $I_{cp} = \frac{5 - E_s - 2.5}{100k} \approx 20\mu A$ in accordance with the `LSU4.9` specifications.

2.2.3 Pump cell electronics

Three functions are necessary to drive the pump cell: first a demodulator converts the micro controller's output to a voltage proportional to the required I_p; this voltage then

---

[3]$R_i \ll 10k\Omega$ for temperatures above 500 °C
[4]recall that E_s can be regulated at 0.45V only when the sensor is hot enough ($T > 650$ °C)
[5]$R_i \ll 100k\Omega$ and $E_s = 0.45V$

feeds a current source; finally, the nominal pump current $I_{p_{nom}}$ is amplified and scaled for AD conversion.

PWM demodulator
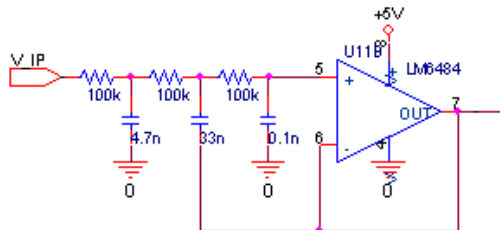
Figure 2.10: pulse-width demodulator consisting of a 3rd order lowpass Chebyshef filter.

The micro controller[6] outputs a PWM signal V_{IP} from 0V to 5V whose modulation frequency f_{PWM} has been fixed to 10kHz. The modulated signal is filtered through an order 3 low pass Chebyshef filter with cutoff frequency equal to 1kHz which gets rid of the PWM's harmonics[7] (corresponding to frequencies kf_{PWM}). A detailed discussion on the choice of the filter parameters is given in Appendix C.1.

I_p current source
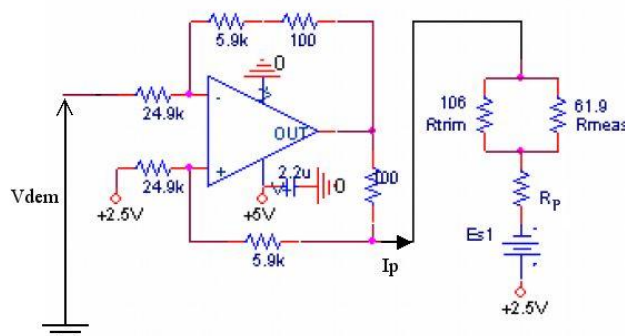
	min	max	typical	
V_{dem}	0V	5V	Air: 0.38V	$\lambda = 1$: 2.5V
I_p	-6mA	6mA	Air: 2.54mA	$\lambda = 1$: 0mA
Operating ratings				
$R_p + R_{cal}//61.9$	0Ω	300Ω	?	
E_p	0V	0.8V	?	

Figure 2.11: Pump current source

The demodulated voltage V_{dem} feeds an active current source wich applies the desired pump current to the pump cell. When connected as on Figure 2.11, the operational

---

[6]Or the output buffer in case of a 3.3V logic micro controller

[7]The amplitude of the nth order component is defined by $2A\tau\text{sinc}(\pi n\tau)$ and the continuous component is $A\tau$, where A denotes the amplitude of the PWM signal (5V), and τ its duty cycle

amplifier outputs a current inversely proportional to the difference between the input voltage and the 2.5V virtual ground:

$$
\begin{aligned}
I_p &= -\frac{6\mathrm{k}}{24.9\mathrm{k} \cdot 100}\left(V_{dem} - 2.5\right) \\
&= -0.0024\left(V_{dem} - 2.5\right)
\end{aligned}
$$

The current source ensures a linear behaviour as long as the operational amplifier does not saturate. It is designed to handle output resistances — composed of the measurement resistance of 61.9Ω, the calibration resistance R_{cal} and the internal pump cell resistance R_p — up to 300Ω and output voltages up to 0.8V.

$I_{p_{nom}}$ measurement
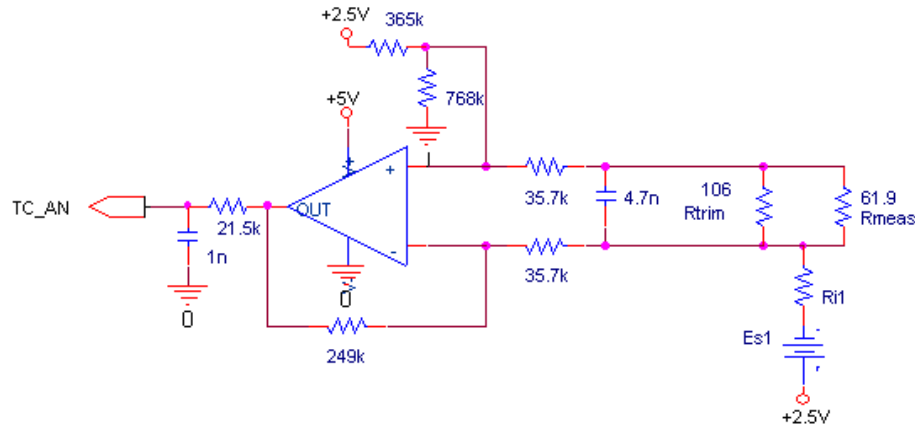
	min	max	typical	
$I_{p_{nom}}$	-4mA	4mA	Air: 2.54mA	$\lambda = 1$: 0mA
V_{ADC}	0V	3.3V	Air: 2.8V	$\lambda = 1$: 1.7V

Figure 2.12: Nominal pump current amplification block

The nominal pump current is computed by measuring the voltage drop accross the 61.9Ω resistor. The operational amplifier of Figure 2.12 amplifies this voltage and shifts it up so that the output completely fits the AD conversion range (0-3.3V in this case). The input-output characteristic is then:

$$
\begin{aligned}
V_{ADC} &= \frac{249\mathrm{k}}{35.7\mathrm{k}}I_{pnom} + \frac{768\mathrm{k}}{768\mathrm{k} + 365\mathrm{k}}2.5 \\
&= 7 \cdot I_{pnom} + 1.7
\end{aligned}
$$

This configuration enables a $I_{p_{nom}}$ measuring range between -4mA and 4mA. Considering the $I_p - \lambda$ characteristic (Appendix B.5), this could seem overdimensioned since the typical measuring range is (-2.22mA..2.54mA) corresponding to $\lambda = (0.65...\text{air})$. However, in this project, the sensor was most of the time tested in free air which implied to extend the measuring range. It remains possible to improve the accuracy by using an amplification gain of 10 for example, corresponding to the typical measuring range $\lambda = (0.65...\text{air})$.

2.3 The Tricore 1796 micro controller

In addition to the development of a wide band oxygen sensors controller, the aim of this internship was to get familiar with a new family of micro controllers, the Tricore series from INFINEON. These processors will be used in the next years ECUs and require some in-depth knowledge of their new functionalities. In this way, the main task of this project was to build an embedded application on the Tricore 1796 micro controller as if it was a complete ECU, using as few electronics as possible to fully control the UEGO sensor.

2.3.1 A brief description of the microcontroller's functionnalities

The TC1796 microcontroller is mounted on a demo board which provides quick accesses to its capabilities. On one side, it has four 80-pin connectors with all the I/O signals of the CPU. On the other side, it is possible to use a serial and a parallel connection to a computer. In this way, a program can be loaded from the computer to an on board memory. The program is first developed in C-language using the Development environment *Tasking*. Then it is compiled and finally sent to the demo board. Fortunately, the architecture of the program can be automatically generated by a Tricore specific software called *Dave*, which configures all the basic CPU registers according to what is needed. Nevertheless, non-basic or more advanced operations require a precise configuration of registers and therefore imply a good knowledge of each component.

Basically, here are the main system units that were used and some useful features:

- the 32-bit CPU working at frequencies up to 150MHz.

- 2MByte of on-chip flash memory.

- an interrupt system with 2*255 hardware priority arbitration levels serviced by the CPU.

- a General Purpose Timer Array module (GPTA) providing a set of timer functionalities to realize autonomous I/O management and to generate complex waveforms like PWM (Pulse Width Modulated) signals.

- a 16-channel Analog-to-Digital Converter unit (ADC) with selectable 8-bit, 10-bit or 12-bit resolution with a conversion time below $2.5\mu s$.

- many digital I/O lines.

- an Asynchronous Serial Channel (ASC), in order to communicate with the computer when a program is running. Information was collected or sent through the Serial port of the computer using NI LabVIEW. A simple LabVIEW interface was developed to collect ADC conversions and to switch modes in the program without interrupting it. A screen shot of this interface is attached in Appendix D.

- a DMA (Direct Memory Access) controller used to transfer data without the intervention of the CPU.

2.3.2 Configuration of the microcontroller

The diagram of Figure 2.13 describes the architecture of the control system based on the TC1796 microcontroller. The strategy consists in using as many external units as possible so as not to overload the CPU. Three main functional units are finally involved:
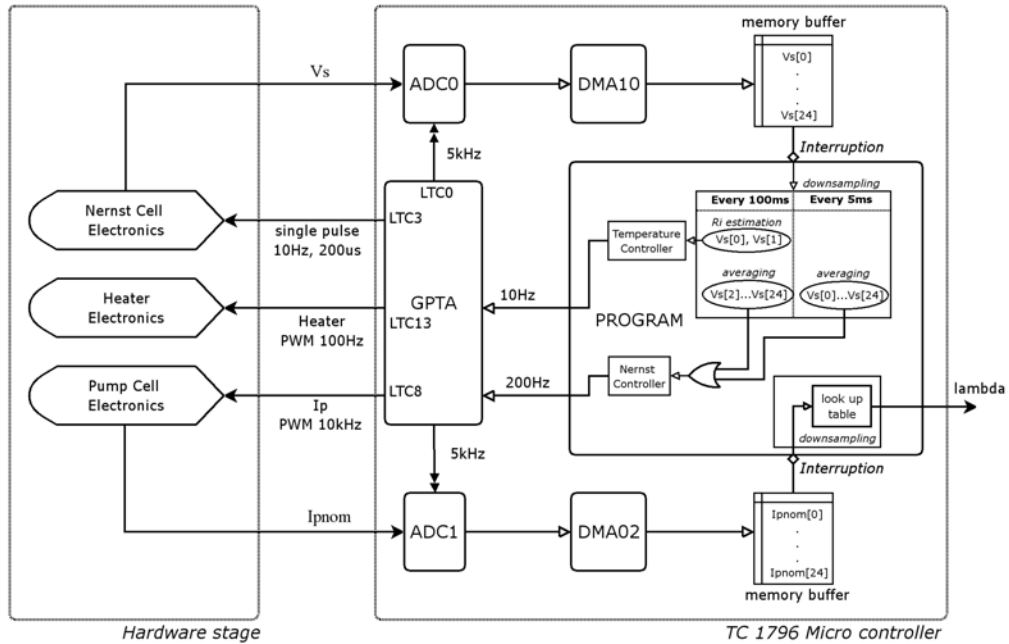
Figure 2.13: Overview of the microcontroller's configuration

The GPTA (General Purpose Timer Array)

The GPTA gathers all the timing components and plays a key role in the synchronization of tasks. It comprises different Local Timer Cells (LTC) that can easily generate PWM signals and trigger other modules. A first set of cells is used to trigger the AD conversions. Another one realizes the temperature measurement pulses. The two last sets are dedicated to the generation of the heating PWM command and the PWM pump current.

Figure 2.14 shows the time instants when the AD conversions occur in comparison with the R_i measurement pulses (previously discussed in section 2.1). LTC0 denotes the timer related to ADC triggering and LTC3 refers to the measurement pulse generation timer. Both timers are incremented with the same input clock. LTC0 is 200μs-periodic whereas LTC3 is 100ms-periodic.

LTC3 is associated to 2 compare units that can generate events when the timer meets some specified values. These compare events occur with a 10μs time delay referring to the ADC time instants and they set/reset a GPTA output. The result is a 10μs-shifted pulse applied to the Nernst cell for R_i measurement. In this way, V_s is clearly measured on top of the pulse as well as just before the pulse.

The ADC (Analog to Digital Converter)

Two separate ADCs are used so that the two variables V_s and I_p can be sampled simultaneously. Both are triggered by a LTC0 timer event at a sampling frequency approximately equal to 5kHz. The signals are sampled over 10bits in comparison with a 3.3V reference voltage.

The DMAC (Direct Memory Access Controller)

A 5kHz Nernst regulation frequency would be too high regarding the sensor's dynamics. The CPU would have to handle too many useless interruptions if such a frequency was
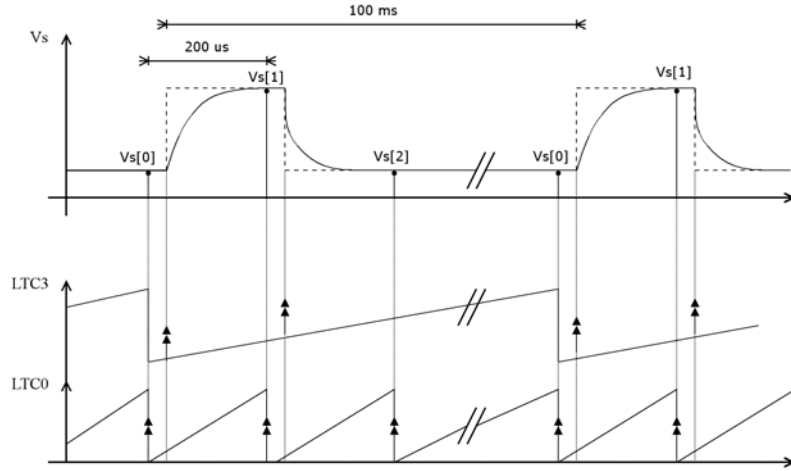
Figure 2.14: Chronogram showing V_s acquisition and timers LTC0 & LTC3

used. Memory buffers and DMAC units are hence used in order to divide the regulation frequency and reduce the measurement noise in the mean time.

The CPU is interrupted only after 25 samples of each signal have been measured and stored into separate memory buffers. This process is equivalent to a downsampling operation from a 5kHz to a 200Hz sampling rate. Two separate DMA channels (DMA10 and DMA02) are involved in the data transfers from the ADCs result registers (ADC0 and ADC1 respectively) to the memory buffers. The DMA transfers are automatically triggered by the ADCs when a new conversion has been realized. The CPU interruptions are finally generated by the DMA as soon as 25 samples have been collected.

A list of the different LTCs, ADCs and DMAs and their respective properties is given in Appendix E.

2.3.3 Software key points

This section describes the way the program computes T, V_s and λ given the different acquisitions realized by ADC0 and ADC1.

Estimation of the temperature T

In its actual configuration, the microcontroller is able to deliver an estimation of the temperature every 100ms. The conversion is achieved using the following relation, derived from the electrical circuit of Figure 2.8:

$$R_i = \frac{10\text{k}}{\frac{5-V_s[0]}{V_s[1]-V_s[0]} - \frac{10\text{k}}{100\text{k}}}$$

where $V_s[0]$ and $V_s[1]$ respectively denote the samples measured just before the measurement pulse and on top of it (see Figure 2.14). Once the internal resistance is measured, the corresponding temperature is computed thanks to the relation $T = f(R_i)$ established in Appendix B.3.

Computation of the Nernst voltage V_s and the nominal pump current $I_{p_{nom}}$

The downsampling operation described previously comes down to an arithmetic averaging of the 25 samples stored in the different memory buffers every 5ms. A more specific

digital filter could have been investigated to increase the SNR. However, taking the arithmetic average results in applying a low-pass filter to the signal which turns out to reduce sufficiently the acquisition noise.

The other advantage of using memory buffers lies in the efficiency in separating the temperature measurement samples from the regular ones. All you have to do is to ignore the two first samples ($V_s[0]$ and $V_s[1]$) every 100ms corresponding to an internal resistance estimation.

Estimation of the AFR λ

The nominal pump current is a picture of the AFR λ as it is represented on the nominal characteristic given in Appendix B.5. In the lean region ($\lambda > 1$), the pump current is almost uniquely determined by the oxygen concentration. This conversion formula can hence be systematically employed to compute the AFR λ:

$$\lambda = \frac{aI_{p_{nom}} + 1}{1 - bI_{p_{nom}}} \quad \text{with} \quad (a = 0.0839, b = 0.3901)$$

In the rich region ($\lambda < 1$), the pump current is strongly dependent on the different gaseous species present in the mixture. The nominal characteristic given in Appendix is only relevant for a precise gaseous composition. In practice, complex models are employed to realize the conversion from $I_{p_{nom}}$ to λ. However, in this study, the lean-region formula is employed in both cases which is not very restricting since the sensor is most of the time studied in the lean region.

Chapter 3

Modelling and controlling the UEGO sensor

From the steady state analysis performed in section 1.3, it appeared that two variables of the UEGO sensor need to be regulated:

- the electrolyte temperature T must be regulated around $780\,°\mathrm{C}$ to ensure a high enough conductivity of the zirconia electrolyte.

- simultaneously, the nernst `EMF` E_s must be adjusted to a reference value of about 450mV in order to obtain the best resolution over λ (see voltage-current characteristic on Figure 1.7).

As a result, two regulation loops are required to run a UEGO sensor: one for the heating process and one for the pump-gauge system.

3.1 Temperature regulation

It is useful to determine a simple model of the sensor since it involves first order thermic phenomena which are easy to model and can help for the design of the optimal temperature controller. The process that is being studied is $T = f(\tau)$, where τ denotes the duty cycle of the heating PWM command.

3.1.1 Open loop analysis

First, the sensor is tested without any feedback using different PWM duty cycles. The time response is represented on Figure 3.1 and leads to these first comments. The system is first order but seems to be slightly nonlinear. For identical input steps amplitudes, the corresponding temperature steps are not constant. This nonlinearity is probably due to the fact that the heating resistance increases with respect to the temperature.

The linear system around the operating point $T_{ref} = 780\,°\mathrm{C}$ is identified from the step response represented on Figure 3.2 and leads to the following first-order transfer function:

$$\frac{\tilde{T}}{\tilde{\tau}} = \frac{835}{1 + 9s} \tag{3.1}$$

3.1.2 Controller design

The methodology consists in designing a continuous controller from the continuous model (3.1) and then discretizing it for software implementation.
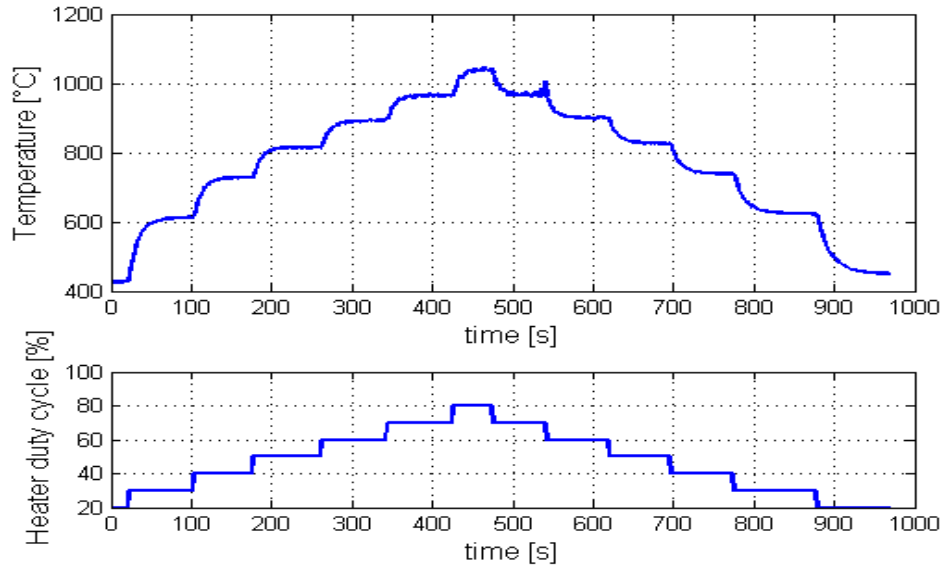
Figure 3.1: Open loop temperature for different duty cycles.
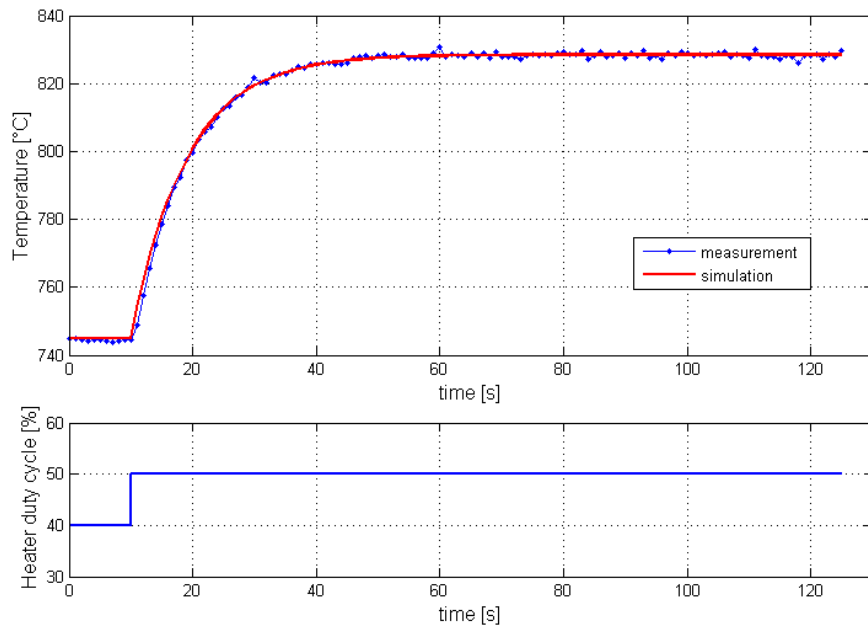
Figure 3.2: Modelled and measured step responses to a 10% duty cycle variation around linearization point. (sampling frequency: 1Hz + averaging)

PI controller

A basic PI controller is investigated here. A simple proportional feedback leads to a permanent static error due to the first-order nature of the system. Therefore, the regulator must include an integral part, as shown on Figure 3.3.
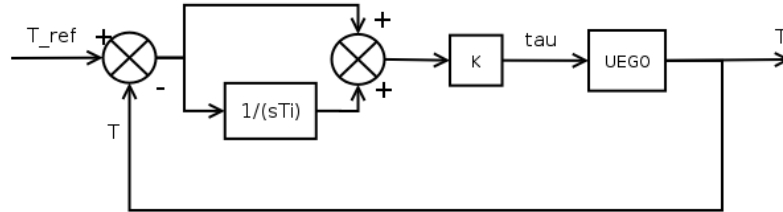

Figure 3.3: Block diagram of the temperature controller

The I-part coefficient is set to the time constant of the system ($T_i = 9$) in order to obtain a first-order closed loop tansfer function[1]:

$$\frac{\tilde{T}}{\tilde{T}_{ref}} = \frac{1}{1 + \frac{9}{835 \cdot K}s}$$

It clearly appears that the response time of the closed loop system is fully-determined by the proportional gain. However, this system is not stricly linear since it includes a saturation of the input duty cycle. It is hence necessary to limit the controller's gain for stability reasons.

A compromise choice between speed and stability finally leads to these PI parameters: $T_i = 9$s and $K = 0.008$. Figure 3.4 shows the step response of the closed loop system. The 0-95% rising time of the compensated system has been reduced to 4s, which is 7 times shorter than the open-loop response time.

Implementation on the microcontroller

The continuous PI-controller transfer function is defined by:

$$\frac{\tau}{\epsilon} = K(1 + \frac{1}{T_i s}) \qquad \text{with} \qquad \epsilon = 780 - T$$

This transfer function is Euler-discretized at the sampling period $T_s = 100$ms to become suitable to software implementation. The heater command is then given by: $u(k) = u_p(k) + u_i(k)$ where

$$
\begin{aligned}
u_p(k) &= K\epsilon(k) \\
u_i(k+1) &= u_i(k) + K\frac{T_s}{T_i}\epsilon(k)
\end{aligned}
$$

The control algorithm is detailed in Appendix F. A particular procedure is engaged when the input τ saturates: the integral part is no more relevant and must consequently be frozen.

---

[1]The open loop transfer function including the compensator is: $\frac{835}{1+9s} \cdot \frac{K}{T_i s}(1+T_i s) = \frac{835K}{9s}$ since $T_i = 9$
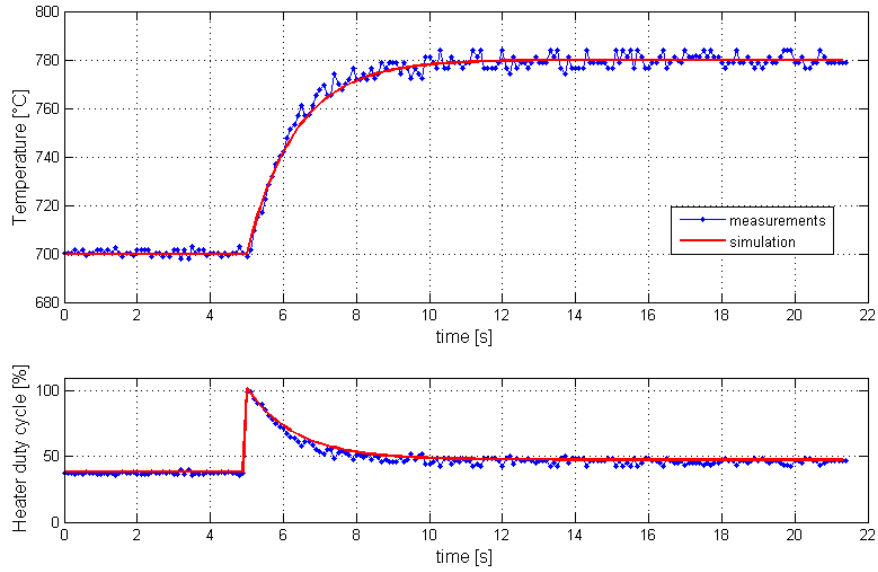
Figure 3.4: Simulated and measured step responses of the closed loop system. (sampling frequency: 10Hz)

3.2   Nernst Voltage regulation

In this control loop, the system to be controlled is a nonlinear process $\dot{E}_s = f(E_s, I_p, P_{O_2})$ which can be reduced to $\dot{E}_s = f(E_s, I_p)$, considering the oxygen partial pressure changes as disturbances. The serial controller, as shown on the block diagram of Figure 3.5, is supposed to regulate the Nernst EMF measurement E_s around 450mV under the best stability and velocity conditions. Precision is not a key point in this particular case since the information about the AFR is not carried by E_s but by the steady state pump current I_p which shows little dependance on E_s around 450mV according to the UEGO voltage-current characteristic (see Figure 1.7).
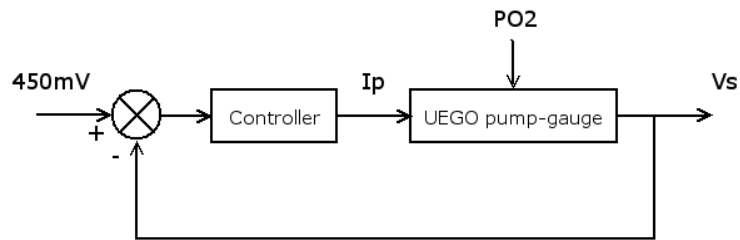
Figure 3.5: Block diagram of the Nernst EMF control system at a given sample gas oxygen partial pressure P_{O_2}.

3.2.1   Measurement of the Nernst `EMF` E_s

Previously, V_s was defined as being the voltage drop at the sensor's outputs (section 2.1.2). Following is a discussion about the difference between the output voltage V_s and the Nernst `EMF` E_s.

When operated at $780\,^\circ\mathrm{C}$, the pump and the Nernst cells are equivalent — as a first order approximation — to a Thevenin voltage source (respectively E_p and E_s) associated with an internal resistance (respectively R_p and R_i). Besides, the internal electrodes in contact with the internal volume are connected as shown on Figure 3.6.
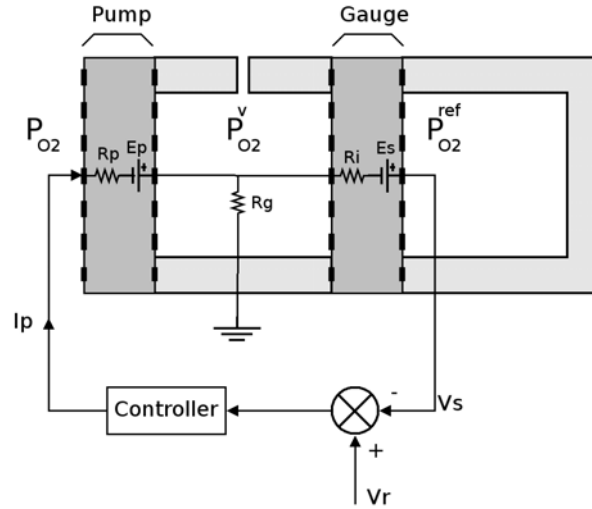

Figure 3.6: Electrical model of the UEGO sensor.

When applying a current I_p to the pump cell, it appears that part of this current circulates through the internal resistance of the Nernst cell R_i, resulting in an additive voltage at the outter Nernst cell electrode:

$$V_s = E_s + R_{cell}I_p \qquad (3.2)$$

where R_{cell} is the Thevenin equivalent resistance of the electrical circuit constituted by the two cells. Even if R_{cell} is so small that $V_s \approx E_s$ in steady state, it may contribute to the sensor's dynamics.

3.2.2   Modelling

In this section, a dynamical model of the UEGO sensor is derived in order to get an idea of the involved dynamics. Linear identification methods work very poorly. The system is indeed strongly nonlinear due to the Nernst relation. Here a physical approach is investigated, trying to describe as simply as possible the pump-gauge reactions taking place between the two cells. The electrochemical reactions are assumed to be instantaneous since this study only focuses on the control mechanisms. This dynamical analysis is performed on the `BOSCH LSU4.9` sensor, ie the pseudo-reference cell sensor, operating in the lean region.

Transient analysis

Let us consider the device of figure 1.6 operating in the lean case, ie with free oxygen remaining. The variation of oxygen inside the internal volume is given by the difference

between the flux of oxygen leaking into the chamber through the diffusion hole and the amount of oxygen pumped out by the applied currents I_p and I_{cp}

$$\frac{\mathrm{d}n_{\mathrm{O}_2}(t)}{\mathrm{d}t} = \sigma_{\mathrm{O}_2}\left(P_{\mathrm{O}_2} - P^v_{\mathrm{O}_2}(t)\right) - \frac{I_p(t)}{4F} - \frac{I_{cp}}{4F} \tag{3.3}$$

The ideal gas equation applied to the internal gas gives

$$\frac{\mathrm{d}P^v_{\mathrm{O}_2}(t)}{\mathrm{d}t} = \frac{RT}{v}\frac{\mathrm{d}n_{\mathrm{O}_2}(t)}{\mathrm{d}t} \tag{3.4}$$

Eliminating $\frac{\mathrm{d}n_{\mathrm{O}_2(t)}}{\mathrm{d}t}$ between equations (3.3) and (3.4) gives finally

$$I_p(t) = -4F\left[\frac{v}{RT}\frac{\mathrm{d}P^v_{\mathrm{O}_2}(t)}{\mathrm{d}t} + \sigma_{\mathrm{O}_2}\left(P^v_{\mathrm{O}_2}(t) - P_{\mathrm{O}_2}\right)\right] - I_{cp} \tag{3.5}$$

$P^v_{\mathrm{O}_2}(t)$ is related to the gauge `EMF` $E_s(t)$ by the Nersnt equation (1.7). Besides, the reference oxygen partial pressure $P^{ref}_{\mathrm{O}_2}$ is given by equation (1.13). (The reference chamber is assumed to be at steady state since I_{cp} is constant).

Eliminating $P^v_{\mathrm{O}_2}(t)$ in (3.5) leads to the following current-voltage relation:

$$\begin{cases} I_p(t) &= -4F\left[P^{ref}_{\mathrm{O}_2}\left(\sigma_{\mathrm{O}_2} - \frac{4Fv}{(RT)^2}\frac{\mathrm{d}E_s(t)}{\mathrm{d}t}\right)\exp\left(\frac{-4F}{RT}E_s(t)\right) - \sigma_{\mathrm{O}_2}P_{\mathrm{O}_2}\right] - I_{cp} \\[2mm] P^{ref}_{\mathrm{O}_2} &= P_{\mathrm{O}_2} + I_{cp}/4F\sigma^{ref}_{\mathrm{O}_2} \end{cases}$$

which can also be written with respect to E_s:

$$\begin{cases} \frac{\mathrm{d}E_s(t)}{\mathrm{d}t} &= \frac{1}{vP^{ref}_{\mathrm{O}_2}}\left(\frac{RT}{4F}\right)^2\left[(I_p(t) + I_{cp} - 4F\sigma_{\mathrm{O}_2}P_{\mathrm{O}_2})\exp\left(\frac{4F}{RT}E_s(t)\right) + 4F\sigma_{\mathrm{O}_2}P^{ref}_{\mathrm{O}_2}\right] \\[2mm] P^{ref}_{\mathrm{O}_2} &= P_{\mathrm{O}_2} + I_{cp}/4F\sigma^{ref}_{\mathrm{O}_2} \end{cases} \tag{3.6}$$

Identification

Equation 3.6 constitutes a complete model of the pseudo-reference `LSU4.9` sensor in the lean region. It is yet wiser to approximate this sensor to a fixed reference oxygen sensor like the `LSU4.2` in order to figure out the leading dynamics. This approximation is possible provided two assumptions: according to Appendix B.4, the reference oxygen partial pressure $P^{ref}_{\mathrm{O}_2}$ is almost constant and equal to $18P^{air}_{\mathrm{O}_2}$ and $I_{cp} \ll I_p$ which leads to the following simplified equation:

$$\frac{\mathrm{d}E_s(t)}{\mathrm{d}t} = \frac{1}{18vP^{air}_{\mathrm{O}_2}}\left(\frac{RT}{4F}\right)^2\left[(I_p(t) - 4F\sigma_{\mathrm{O}_2}P_0X_{\mathrm{O}_2})\exp\left(\frac{4F}{RT}E_s(t)\right) + 4F\sigma_{\mathrm{O}_2}18P_0X^{air}_{\mathrm{O}_2}\right] \tag{3.7}$$

One should note that instead of dealing with oxygen partial pressures $P^i_{\mathrm{O}_2}$, the corresponding oxygen concentrations $X^i_{\mathrm{O}_2}$ are considered, which is more convenient. For a given gas at the atmospheric pressure $P_0 = 1013\text{hPa}$, the corresponding oxygen concentration is simply obtained by: $X^i_{\mathrm{O}_2} = P^i_{\mathrm{O}_2}/P_0$.

Some coefficients can not be measured, like the internal volume of the device v and the leak conductance σ_{O_2}. A semi-physical approach based on this equation is hence performed so as to identify the unknown parameters. First, let us re-write equation (3.7) in the standard explicit form, the unknown parameters being collected in the vector θ:

$$\begin{aligned} \dot{E}_s &= f(E_s, I_p, \theta) \\ V_s &= g(E_s, I_p, \theta) \end{aligned}$$

According to (3.7), this gives the following state-space model:

$$\begin{aligned}
\dot{E}_s &= \theta_1 \left[(I_p - \theta_2 X_{O_2}) e^{\theta_3 E_s} + 18\theta_2 X_{O_2}^{air} \right] \\
V_s &= E_s + \theta_4 I_p
\end{aligned}
\qquad \text{with} \quad
\begin{cases}
\theta_1 &= \frac{1}{18 v P_{O_2}^{air}} \left(\frac{RT}{4F} \right)^2 \\
\theta_2 &= 4F \sigma_{O_2} P_0 \\
\theta_3 &= \frac{4F}{RT} \\
\theta_4 &= R_{cell}
\end{cases}$$

Most of the model parameters can be determined through various measurements or right from their definition:

- the resistance R_{cell} is measured by applying a current step to the sensor and measuring the corresponding voltage jump. $R_{cell} \approx 8.5\Omega$

- θ_2 can be estimated by considering the specifications of the UEGO sensor being used. The nominal characteristic given in Appendix B.5 establishes a linear relation between the nominal pump current $I_{p_{nom}}$ and the oxygen concentration in lean gas mixtures: $I_{p_{nom}} \approx 0.012 X_{O_2}$. On the other hand, the theoretical expression of the steady state pump current can be approximated to: $I_p \approx 4F\sigma_{O_2} P_0 X_{O_2}$ according to equation (1.8). Comparing both expressions[2] results in $\theta_2 \approx 0.019$ [SI].

- $\theta_3 = 4F/RT = 44.6$ [SI], assuming that T is regulated around $780\,°C$

- θ_1 is the only parameter that cannot be estimated thanks to measurements since it depends on the volume of the internal pump chamber which is not easily accessed. Most of the identification work consequently concerns the estimation of θ_1. An open loop identification is performed by applying different pump current steps to the sensor and θ_1 is tuned until the model output fits the real system output (see Figure 3.7).

The model parameters are hence:

$$(\theta_1 = 5, \theta_2 = 0.019, \theta_3 = 44.6, \theta_4 = 8.5) \qquad \text{[SI]} \tag{3.8}$$

Model Implementation

Due to the strong nonlinearity of the plant, a Simulink model is derived from the previously established state space model and its related parameters (3.8). A picture of how this model is realized with Simulink is given in Appendix G. It is build around a differential equation editor (`dee`) that can handle any state space model written under the explicit form.

The choice of the numerical solver is important in this case because the plant contains variable dynamics: the gain varies according to $e^{\theta_3 E_s}$ meaning that the system time constant decreases exponentially as the Nernst `EMF` increases. Variable-step stiff solvers are suitable for these kinds of problems and show much better results than fixed-step solvers.

Figure 3.8 is an illustration of this phenomenon: the Simulink model is closed-loop controlled by a PI controller whose coefficients are roughly fixed to ($K = 0.01$ and $T_i = 0.15$). The Nernst Voltage V_s as well as the nominal pump current $I_{p_{nom}}$ are plotted when the reference voltage jumps from 0V to 0.45V under three different oxygen concentrations. In order to check the coherence between the model and the real system, the same PI controller is implemented on the micro controller[3] and the modelled signals are compared with the measurements.

The stiffness of the plant clearly appears on the simulations: when the Nernst EMF reaches a certain value ($\approx$ $0.2V$) the system reacts much faster with a much higher

---

[2] and considering the calibration relation $I_{p_{nom}} = \frac{R_{cal}}{61.9 + R_{cal}} I_p$

[3] the following section explains how this is done
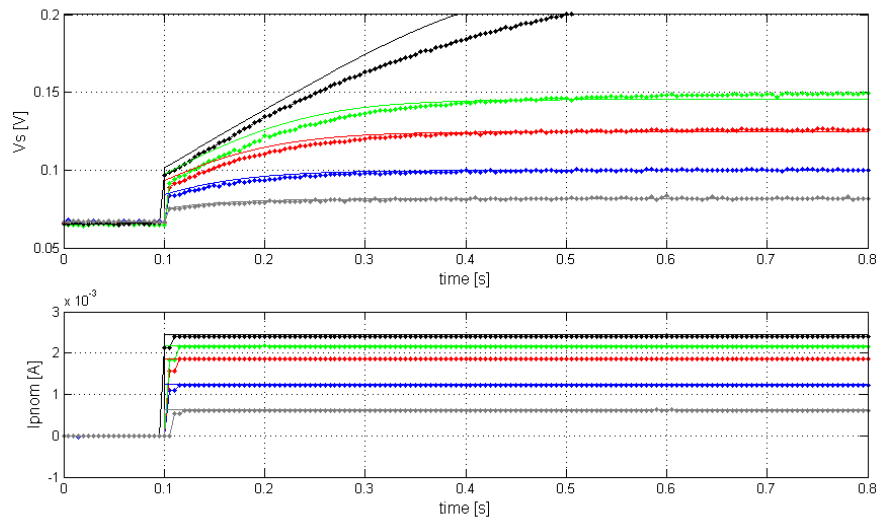
Figure 3.7: Simulated and measured open loop step responses.
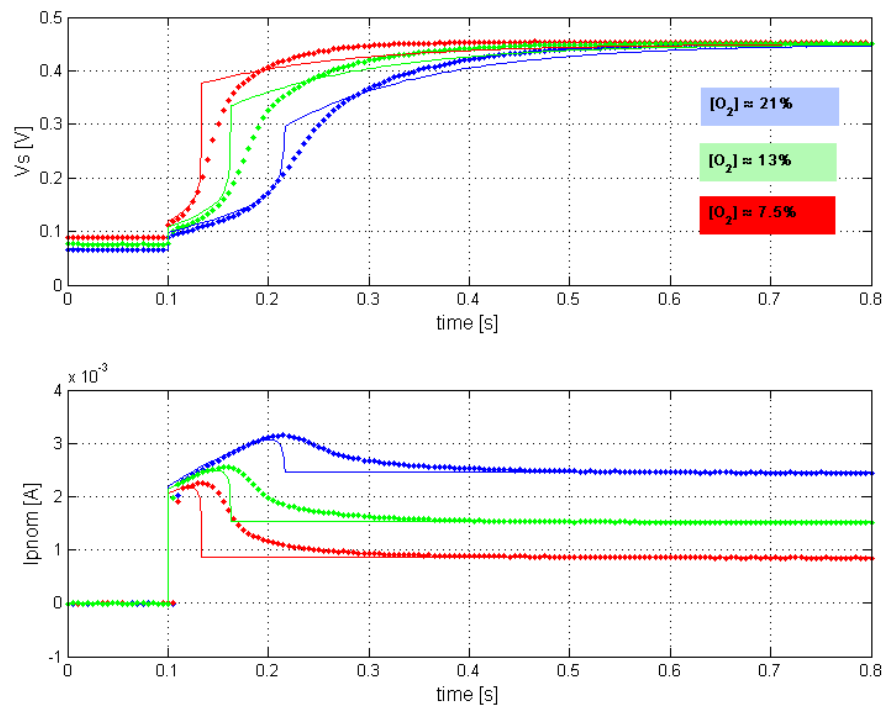
Figure 3.8: Simulated and measured step responses for a reference Nernst voltage jump (0V to 0.45V) under different oxygen concentrations.

gain. At last, the regulation is governed by the integral part of the PI-controller which explains why it turns slower at the end. The real plant fortunately does not show such stiff dynamics probably due to the fact that the electrochemical reactions are not instantaneous in reality.

Figure 3.8 reveals another interesting aspect of the sensor's behaviour: the amount of oxygen within the sample gas governs the settling time of the system. The higher the oxygen concentration, the longer it takes to stabilize the pump current. The system needs indeed to pump a larger amount of oxygen out of the diffusion chamber before a stoichiometric mixture is reached.

3.2.3 Design of the controller

Now that a model of the sensor has been establihed, a PI controller is designed in continuous time and then discretized for software implementation. What distinguishes this control system from the previous one dedicated to temperature regulation is that the variable of interest is the input pump current since it is a picture of the AFR. The precision of the input is therefore a key point in this analysis as well as the plant response to a step disturbance.

PI controller

A PI feedback loop is investigated, as shown on Diagram 3.9. Even though the system is strongly nonlinear, such a linear controller offers good regulation properties.
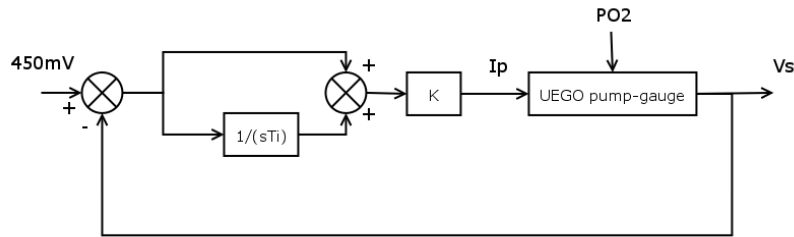

Figure 3.9: Block diagram of the Nernst voltage regulation system

The PI parameters K and T_i are chosen by considering the response of the Simuling model to a step variation[4] of the oxygen partial pressure P_{O_2} depicted on Figure 3.10. This disturbance first results is a deviation of the Nernst voltage V_s from the reference 0.45V. The PI controller then brings V_s back to equilibrium. It seems that K governs the amplitude of the voltage deviation whereas T_i affects the response time of the regulation.

A compromise choice between precision of the pump current and control performance leads to these values: $K = 0.02$ and $T_i = 0.15$.

Implementation on the microcontroller

Like in the temperature control loop, the PI controller is Euler-discretized at the sampling period $T_s = 5$ms to become suitable for software implementation. The pump current command is then given by: $u(k) = u_p(k) + u_i(k)$ where

$$u_p(k) = K(0.45 - V_s(k))$$
$$u_i(k+1) = u_i(k) + K\frac{T_s}{T_i}(0.45 - V_s(k))$$

---

[4]The step disturbance is first low pass filtered to introduce a 50ms settling time, as observed in measurements
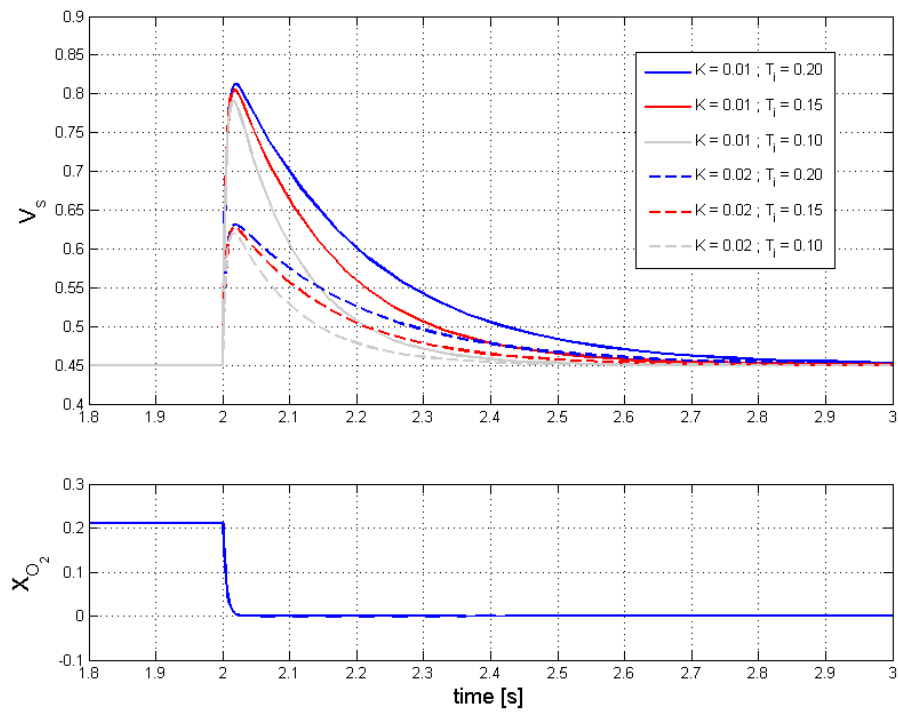
Figure 3.10: Time responses to a step variation of X_{O_2} (from 0.21% to $\approx 0\%$) for different (T_i, K).

The same control algorithm as for the temperature regulation is implemented on the microcontroller (see Appendix F). A particular anti-windup procedure is engaged when the input I_p saturates ($|I_p| > 6$mA): the integral part is no more relevant and must consequently be frozen.

Response to an oxygen concentration step

Figure 3.11 shows the sensor's response to a drop in oxygen concentration . This experiment consisted in blowing some CO_2 inside a small cap mounted on the sensor's head[5]. In this way, it was possible to fully or partially remove the oxygen contained in the cap.
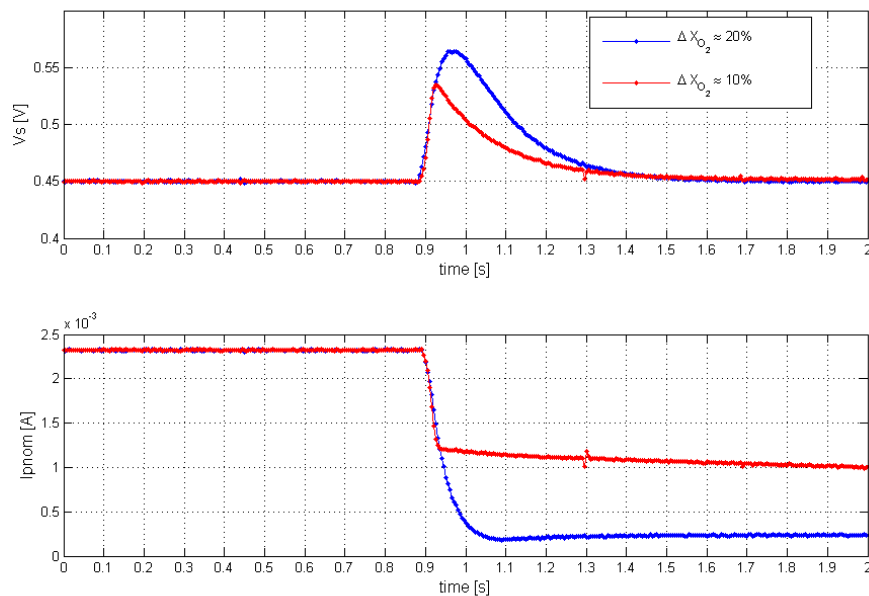
Figure 3.11: Step variations of the oxygen concentration.

In accordance with the simulations, the Nernst voltage V_s is stabilized after 400ms if the oxygen contained in the cap is totally removed. However, the system time response is only about 100ms since the pump current reaches its final value earlier than V_s. This can be explained by considering the sensor's current-voltage characteristic of Figure 1.7. It shows that the sensor outputs the same final current provided that the Nernst EMF is in the neighbourhood of 0.45V.

---

[5]CO_2 is neutral with regards to the sensing element.

Chapter 4

Results

The control system of the UEGO sensor has been developped and tested under atmospheric conditions which were limiting mainly for two reasons:

- regarding the temperature, the sensor is usually immersed in fast and hot exhaust gases which might have an influence on the regulation properties.

- concerning the electrochemical aspect, the sensor has only been tested in the lean region. The control system is designed to handle rich compositions containing reducing species like CO or H_2 but it has not been tested yet.

This section presents the different experiments that have been carried out to test the sensor under more realistic conditions.

4.1   Start-up phase

It is first interesting to observe the sensor's behaviour during an initialisation procedure. The state of the sensor is depicted on Figure 4.1 through its three main variables : V_s, T and $I_{p_{nom}}$.

The temperature is measured only after 4s, at the end of the heat-up phase (see the heat-up profile on Figure 2.4), when the internal resistance becomes measurable. The control system is then activated and drives the temperature to $780\,°C$.

At the same time, as the electrolyte temperature increases and becomes more conductive, the Nernst voltage falls from 1.2V down to almost zero. The Nernst voltage control system is enabled when the temperature reaches $650\,°C$ according to the specifications. Right after this moment, oxygen is pumped out of the diffusion chamber and V_s is stabilized at a constant 0.45V. The overall intitialisation time is about 7s, which is coherent with the performance of the other available control systems.

4.2   Temperature regulation performance

The sensor is tested under more realistic conditions regarding temperature, ie at higher external gas temperature and speed. The experimental setup is represented on Picture 4.2. A hot air blower (also called a Leister) is connected to one of the extremities of a 1-meter long tube on which the UEGO sensor is mounted. A thermocouple measures approximately the gas temperature close to the sensor. The experimental conditions are approximately $(v_{gas} \approx 1.3\text{m/s}$ and $T_{gas} \approx 250\,°C)$[1]

---

[1]According to the Leister specifications, the maximum flow is $D_{gas} = 230\text{L/min}$ and the tube section S is about 28cm^2, yielding $v_{gas} = \frac{D_{gas}}{S} = 1.35\text{m/s}$
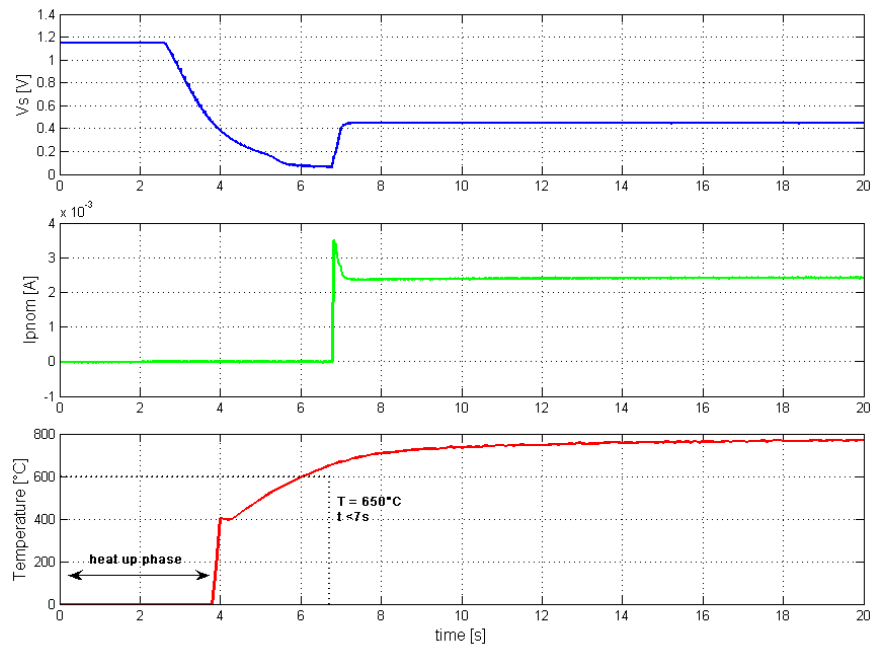
Figure 4.1: Sensor's behaviour during a start-up phase.($v_{gas} \approx 0$m/s and $T_{gas} \approx 25\,°$C)
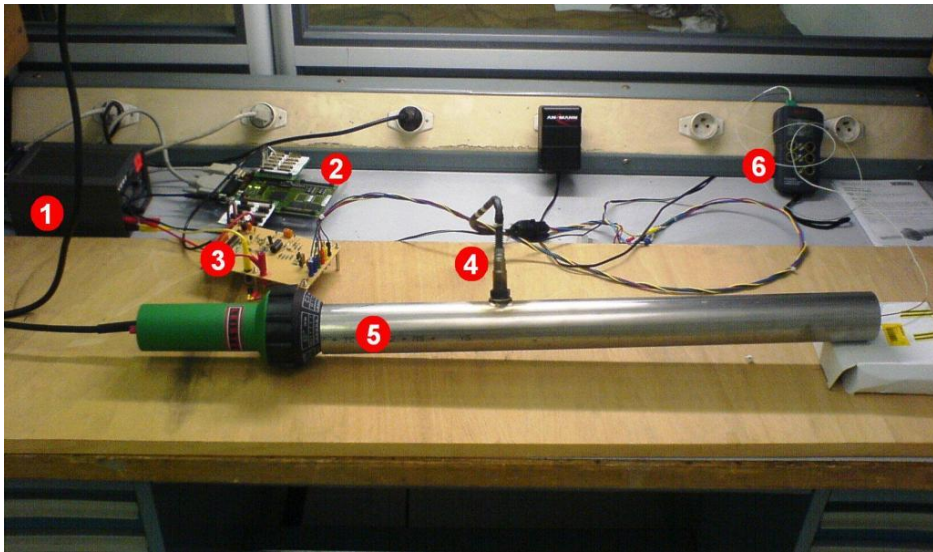
Figure 4.2: Test of the temperature regulation : experimental setup (1: 12V power supply; 2: Tricore 1796 DemoBoard; 3: electrical interface; 4: UEGO sensor; 5: hot air blower (Leister); 6: thermometer)

Figure 4.3 depicts the sensor's response to a step variation of the reference temperature from $700\,°$C to $780\,°$C. The output of the model obtained under atmospheric conditions is also represented to compare the two cases. There is nearly no difference between the results under "atmospheric" conditions and the results with fast and hot gas flow. It seems that the heating system is so close to the the sensing element that it does not depend on external disturbances.
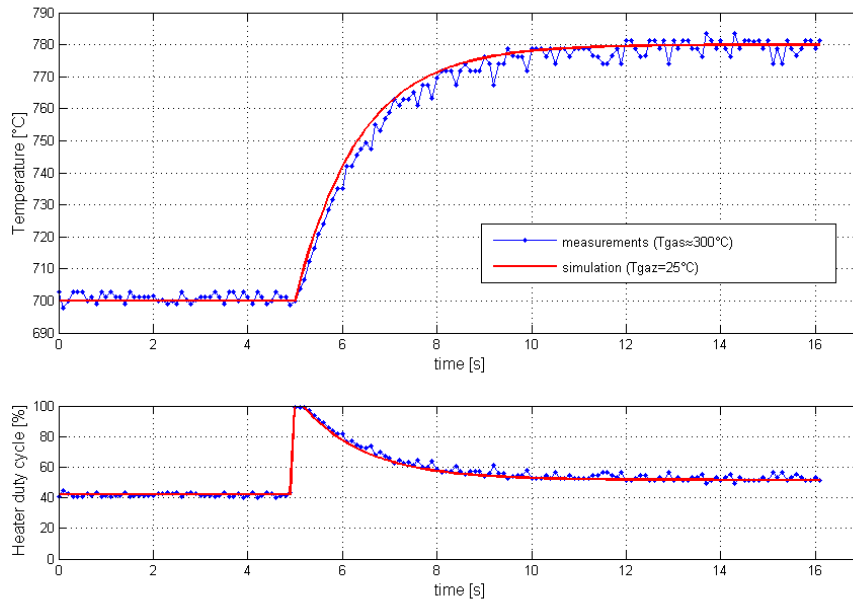
Figure 4.3: Measured step response of the closed loop system with ($v_{gas} \approx 1.3$m/s and $T_{gas} \approx 250\,°$C) and simulated response with($v_{gas} \approx 0$m/s and $T_{gas} \approx 25\,°$C)

4.3 AFR measurement

A lot of uncertainties concerned the behaviour of the sensor in the rich region, where there is no oxygen remaining. RENAULT has a test bench dedicated to experimentations on oxygen sensors which enables the generation of typical exhaust gas compositions. I was given a time slot on this bench in order to qualify this control system. The complete results are given in Appendix H and they are summarized in this section.

Figure 4.4 shows the sensor's response to an AFR step from lean to rich. It gives an idea of how the sensor behaves in the rich region as well as how fast it reacts to AFR step variations. The gaseous composition that is used is a typical exhaust gas composition encountered in Diesel engines. The richness is defined as the inverse of the normalized AFR:

$$r = \frac{1}{\lambda}$$

A richness step from 0.5 to 1.05 hence corresponds to a λ step from 2 to 0.95.

Fortunately the sensor delivers a negative pump current in the rich mixture which means that it reacts to reducing species like CO and H_2 and hence enables the detection of rich AFRs. Besides, the system measures a coherent richness with regards to what was approximately exptected[2].

Concerning the sensor's dynamics, the 10 to 90% settling time is about 50ms which is satisfactory compared to the other available control systems.

---

[2]the compositions generated by the gas bench were not calibrated and could only lead to a qualitative analysis.
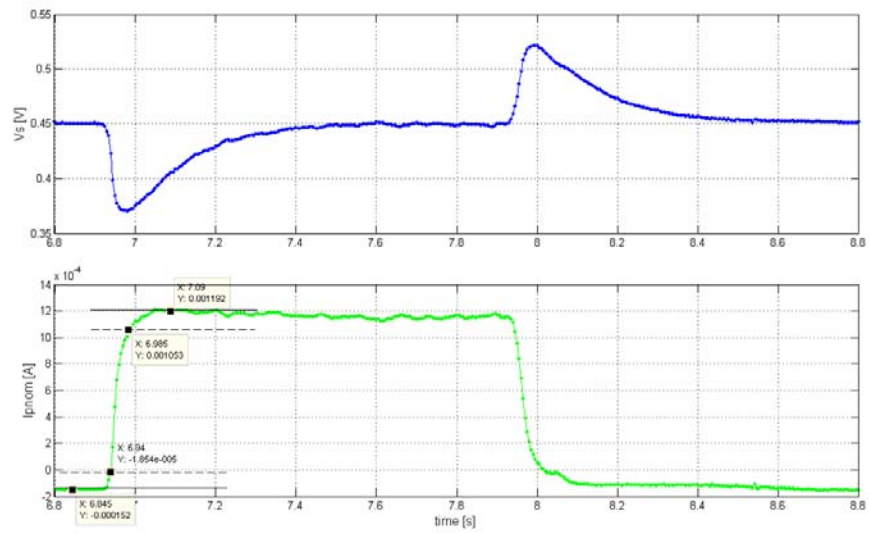
Figure 4.4: Richness step from 0.5 to 1.05.

Conclusion

This project has demonstrated the feasibility of controlling a UEGO sensor directly from a microcontroller, with a low level of cost and complexity. The use of a micro controller is particularly adequate for this application. The two regulation loops are indeed easily implemented on the microcontroller and interferences are immediately removed by software. Conversely, fully-electronic solutions are strongly limited by this overlaping phenomenon occuring between the two control loops.

The main advantage of such a solution lies in the simplification of the electronics. Only basic components are required since all the regulation tasks are handled by the microcontroller. Regarding the precision of the measurements, the addition of discrete-time filtering results in a general improvement of the signals accuracy. The CPU load is minimized because external units (like the GPTA, DMA) have been used as much as possible to reduce the number of CPU interruptions. According to INFINEON to whom this project has been presented, the requirements for this control system are negligeable compared to the Tricore microcontrollers capabilities.

Two PI controllers have been used for the two regulation loops. The temperature controller ensures a stable $780\,^{\circ}$C at the sensing element whatever the outside thermic conditions might be. Regarding the electrochemical regulation, the PI controller has been designed from a dynamical model of the pump-gauge association in the lean region. The gas bench results were coherent even in the case of rich AFRs. This control system has shown satisfactory dynamic and precision performances compared to fully-electronic solutions.

A more advanced application to vehicles is conceivable provided many extra studies: several dissipation phenomena were not taken into account and become critical in vehicle-environments. However, this should not be problematic in this case. All these corrections are usually treated by the engine ECU. This control system is hence much more convenient than any other electronic solution in that the device is directly driven by the ECU.

Appendix A

Exhaust gas composition
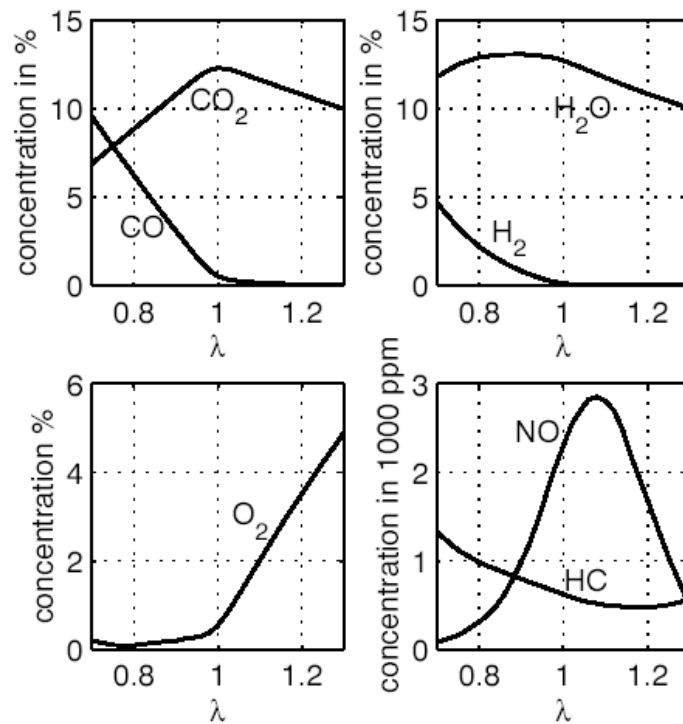
Appendix B

BOSCH LSU4.9 UEGO sensor.

B.1 Cross section of the sensing element
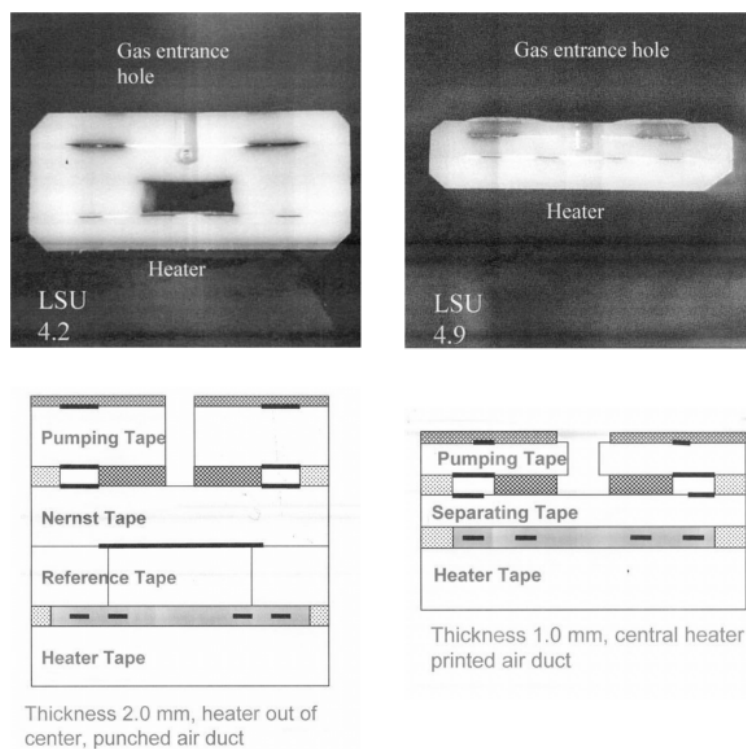
Figure B.1: Cross section of LSU4.2 (left) and LSU4.9 (right) sensing elements.

One should note that the reference chamber does not appear on the cross section of the LSU4.9 sensor. This is due to the fact that it is not located on the same plane as the rest of the sensing part.

B.2 Nominal pump current $I_{p_{nom}}$
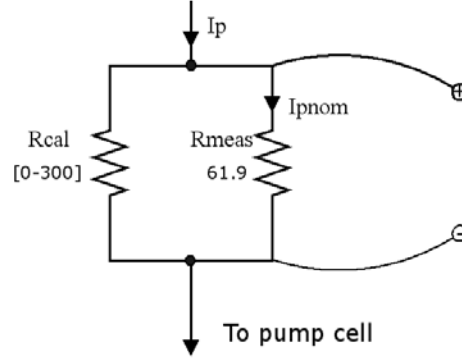
Figure B.2: Calibration resistance and nominal pump current.

Instead of measuring the whole pump current I_p going through the pump cell, the fraction of current $I_{p_{nom}}$ going through $R_{meas} = 61.9\Omega$ is measured. Nominal and effective pump currents are linked together by the following relation:

$$I_{p_{nom}} = \frac{R_{cal}}{61.9 + R_{cal}} I_p$$

B.3 Temperature dependency of the sensor

Nernst-cell internal resistance R_i

The $R_i = f(T)$ characteristic is represented on the following plot. A computational curve-fitting method gives the following logarithmic relation:

$$T = \frac{1}{\gamma} \ln\left(\frac{R_i - \gamma}{\alpha}\right) \qquad \text{with} \begin{cases} \alpha &=& 2.0796 \cdot 10^5 \\ \beta &=& 8.6717 \cdot 10^{-3} \\ \gamma &=& 55.164 \end{cases}$$

Temperature dependency of the sensor signal

The sensor output also varies with respect to temperature changes. According to the sensor specifications, a temperature change gives a deviation of the nominal pump current:

$$\frac{\Delta I_{p_{nom}}}{I_{p_{nom}}} = 4\%/100\,^{\circ}\mathrm{C}$$
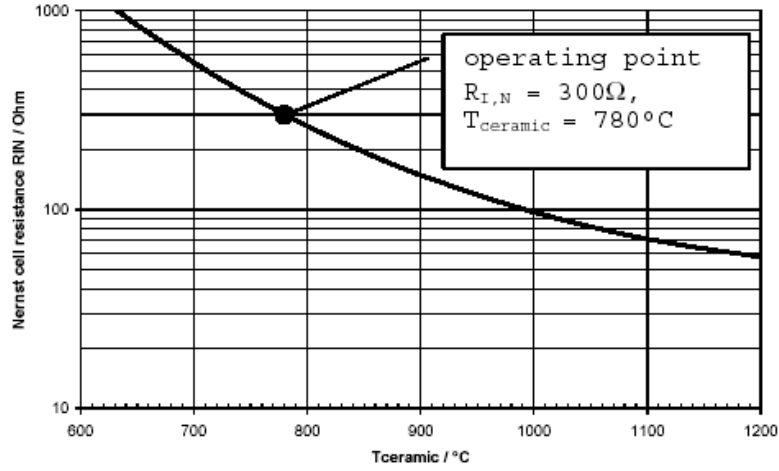
Figure B.3: Nernst cell resistance with respect to the internal temperature

B.4 Pseudo-reference oxygen partial pressure $P_{O_2}^{ref}$

The `LSU4.9` UEGO sensor is an amperometric oxygen gas sensor with pseudo-reference gas (see section 1.3.2) in opposition to the `LSU4.2` which has a stable reference air. In order to maintain excess oxygen within the reference chamber, a constant reference pump current I_{cp} is applied to the reference Nernst electrode. The provision of a small diffusion path balances the oxygen reference partial pressure around a value close to:

$$P_{O_2}^{ref} = P_{O_2} + I_{cp}/4F\sigma_{O_2}^{ref}$$

$I_{cp}/4F\sigma_{O_2}^{ref}$ corresponds to the partial pressure of oxygen pumped into the reference chamber. Its numerical value can be estimated when the sensor is immersed in free air and when no oxygen is pumped into the pump chamber ($I_p = 0$). Under such conditions, $P_{O_2} = P_{O_2}^{v} = P_{O_2}^{air}$ and the gauge `EMF` is given by:

$$E_s = \frac{RT}{4F}\ln\left(\frac{P_{O_2}^{ref}}{P_{O2}^{air}}\right)$$

A Nernst potential of 67mV hence corresponds to a reference partial pressure $P_{O_2}^{ref} \approx 19P_{O2}^{air}$, which leads to

$$I_{cp}/4F\sigma_{O_2}^{ref} \approx 18P_{O2}^{air}$$

The fraction of oxygen pumped in by I_{cp} is consequently much higher than the fraction leaking through the diffusion path. As a result, $P_{O_2}^{ref}$ can be considered to be almost independent on the measured partial pressure P_{O_2}:

$$\begin{aligned} P_{O_2}^{ref} &\approx I_{cp}/4F\sigma_{O_2}^{ref} \\ &\approx 18P_{O2}^{air} \end{aligned}$$

B.5   Nominal characteristic line

| O_2-conc. x_{O2}/%						3.0	6.0	8.29	12.0	20.95
λ-value	0.65	0.70	0.80	0.90	1.013	1.18	1.43	1.70	2.42	air
$I_{p,meas}$/mA	-2.22	-1.82	-1.11	-0.50	0.00	0.33	0.67	0.94	1.38	2.54
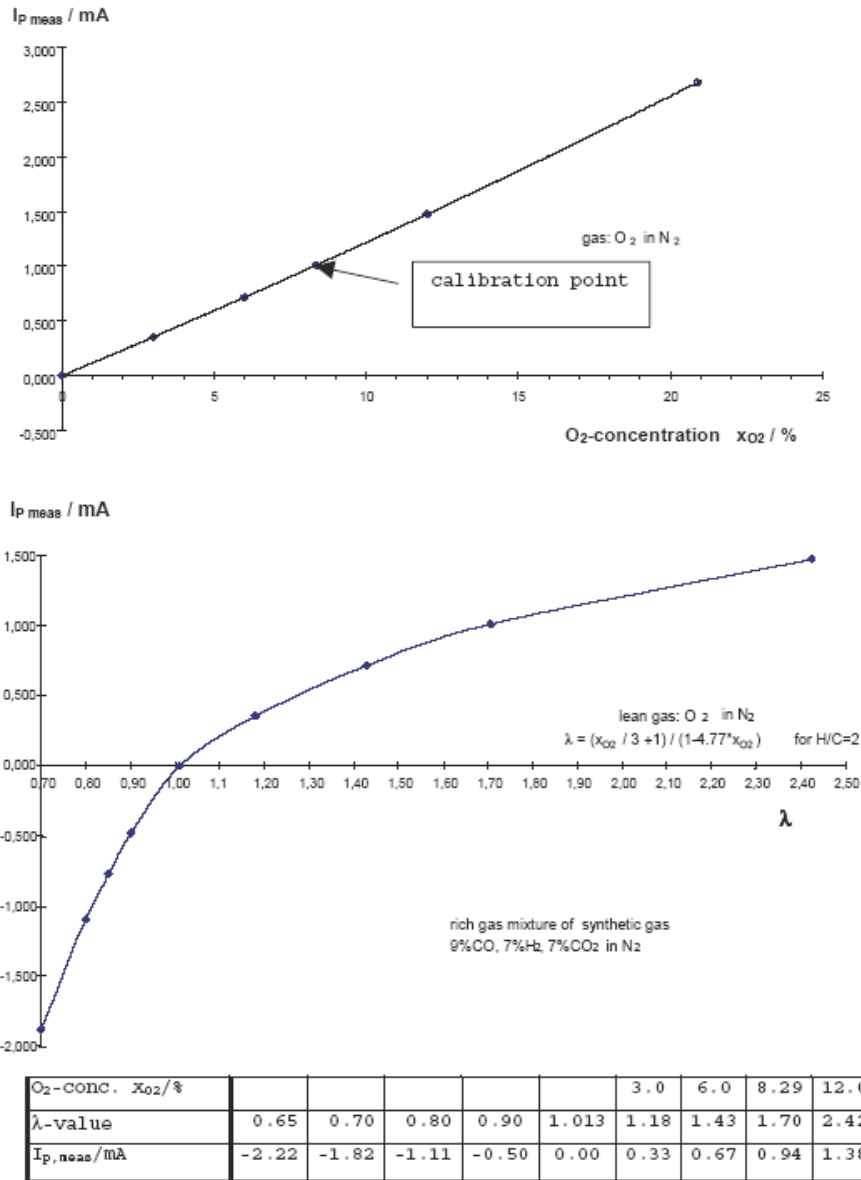
Figure B.4: Nominal output current for various oxygen concentrations and AFR.

Appendix C

Electronic design

C.1 PWM demodulation filter

C.1.1 Choice of the proper filter

A Fourier series decomposition of the modulated signal reveals that the amplitude of the nth order component is $2A\tau\text{sinc}(\pi n\tau)$ and the continuous component is $A\tau$, where A denotes the amplitude of the PWM signal (5V), and τ its duty cycle. The idea is to keep the continuous component which carries the information about the pump current level τ. The cutoff frequency must consequently be chosen as low as possible to maximize the attenuation at the PWM frequency. However, the system's velocity strongly depends on the filter's bandwith. According to the specifications, the time response of the pump current I_p is around 50ms. Hence, the filter's cutoff frequency should not go below 1kHz to guarantee a fast enough system.
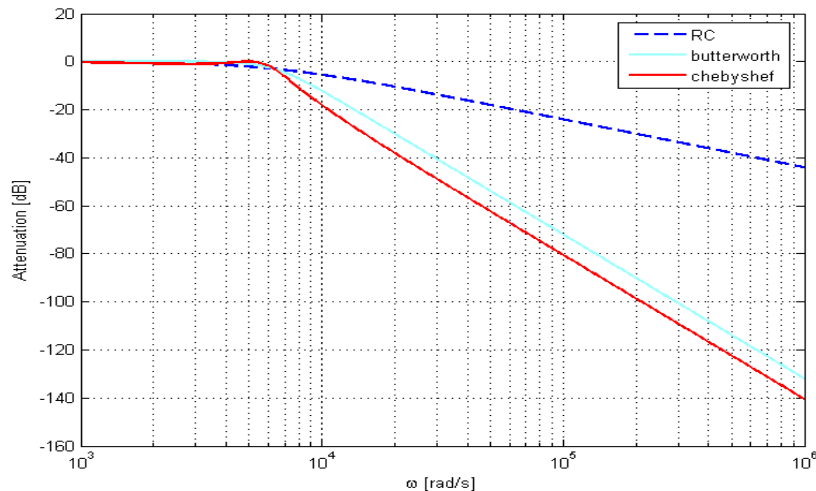
Figure C.1: Bode diagram of different lowpass filters (cut-off frequency 1kHz)

The graph above (see Figure C.1) is a Bode diagram of 3 different filters that have been experimented: a simple RC filter, a 3rd order Butterworth filter and a 3rd order Chebyshef filter. The Chebyshef filter has better attenuation properties than the Butterworth filter. The only drawback of such a filter is the fact that its magnitude is not monotonous inside the bandwidth contrary to the Butterworth filter. However in this application, only the

DC component of the PWM signal cares. Therefore, a Chebyshef filter is the best choice here.

In order to evaluate the final precision on the normalized `AFR` λ, the modulation noise is assumed to be mostly carried by the PWM's fundamental component. Thanks to the $I_p - \lambda$ characteristic, the impact on the final precision can then be derived for different PWM frequencies. The following plots (see Figure C.2) are based on a 50% duty cycle. First, it clearly appears that the higher the PWM frequency is, the higher the attenuation becomes and thus, the better the precision. If a RC filter was used, one would have to use a PWM frequency higher than 100kHz to get a precision below 1% whereas for a Chebyshef filter, the precision is less than 1% at a 10kHz PWM frequency.
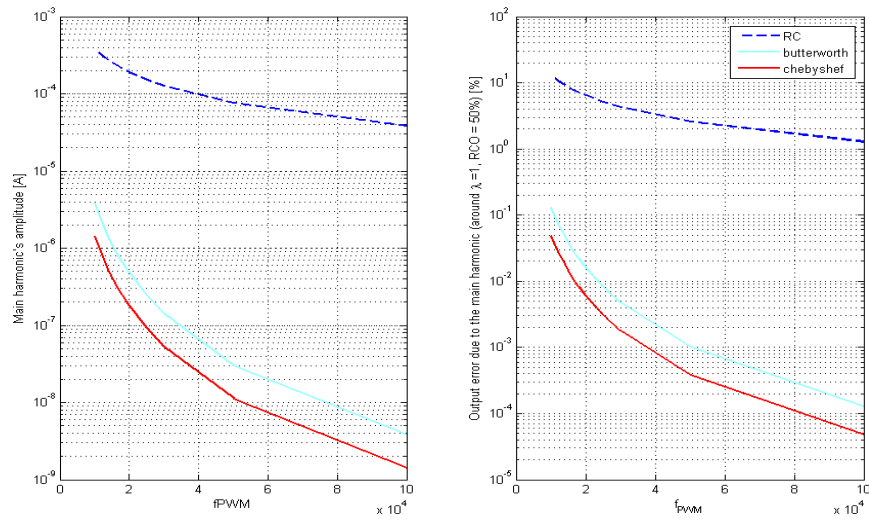
Figure C.2: `AFR` error due to PWM demodulation for different PWM frequencies

C.1.2 Electronic realization

The analog filter design is based on a Sallen-Key structure [6] represented on Figure C.3. Given the cutt-off frequency, the values of the capacitors can be found on tables for each type of filter (Chebyshef, Bessel or Butterworth) and up to order 10. Let f_0 denote the cutt-off frequency and R be the common resistor. The three capacitances are then given by:

$$C_i = k_i C_0 \quad \text{with} \quad C_0 = \frac{1}{2\pi f_0 R}$$

the coefficients k_i depending on the type of filter being designed. For a Chebyshev filter, $k = (16.18, 2.567, 0.0643)$ and for R=100kΩ, $C = (25.75\text{nF}, 4.08\text{nF}, 0.1\text{nF})$. Normalised values are $(33\text{nF}, 4.7\text{nF}, 0.1\text{nF})$.
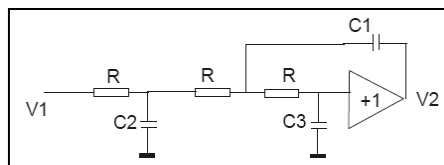
Figure C.3: 3$^{\text{rd}}$ order Sallen-Key cell.

## C.2 Circuit Layout
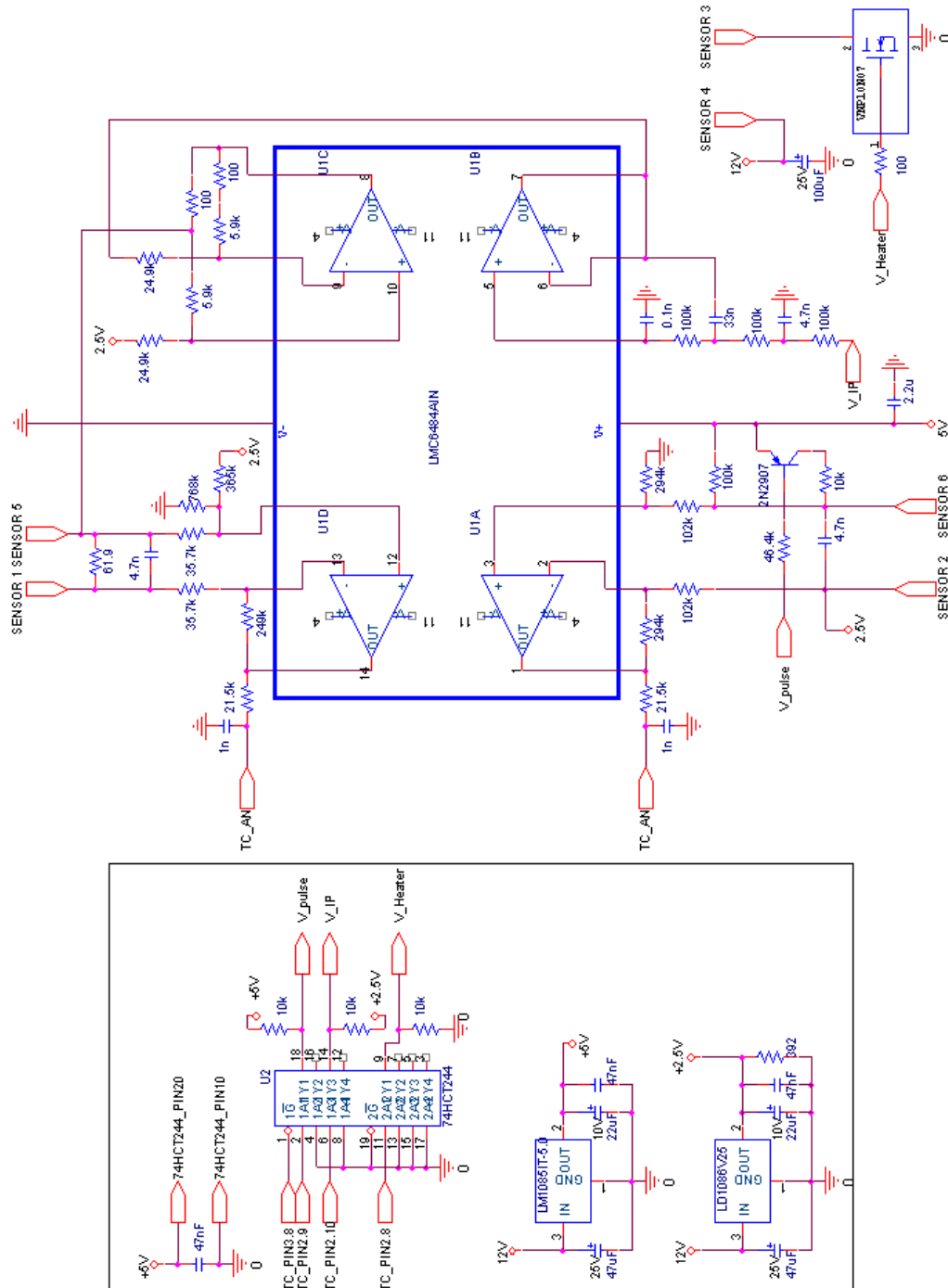
Appendix D

LabVIEW interface for data acquisitions

During this project, visualizing the different signals involved in the control system was a major issue. In order to know precisely the system state variables as they were handled by the microcontroller, the different A/D conversions were periodically sent to a computer via a serial connection. This implied the use of an ASC unit on the microcontroller side and the development of an ASC data reception interface on the computer side.

The data acquisition software LabVIEW has been used for this purpose. The baud rate of the serial transmission was set to 115200 baud, so that every 32-bit sample[1] could be sent in less than 0.5ms by the microcontroller. It was indeed essential not to disturb the time-scheduled control operations of the main program.

Following are two screenshots of the LabVIEW interface which is divided into three tabs:

- the first tab is devoted to configuration parameters.

- the second tab (see Figure D.1) plots the temperature samples in real-time every 10ms.

- the third tab (see Figure D.2) plots all the electrochemical samples (V_s and $I_{p_{nom}}$) which are continuously received by the microcontroller every 5ms. The conversions of the pump current to a λ value first and then to an oxygen concentration value are realized by the LabVIEW program.

---

[1] the microcontroller uses floating point values encoded over 32 bits
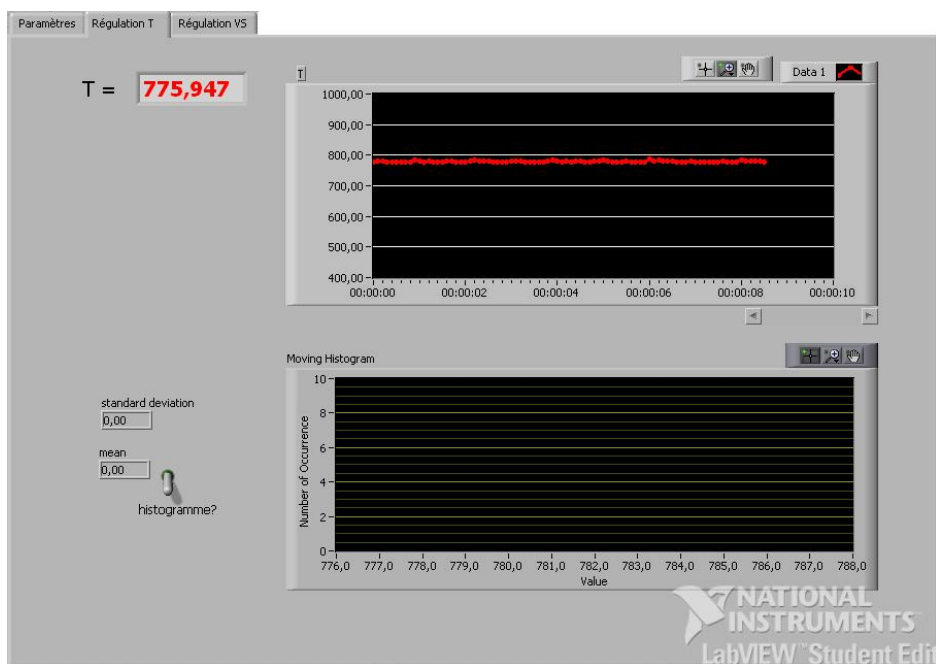
Figure D.1: Screenshot of the temperature acquisition tab.
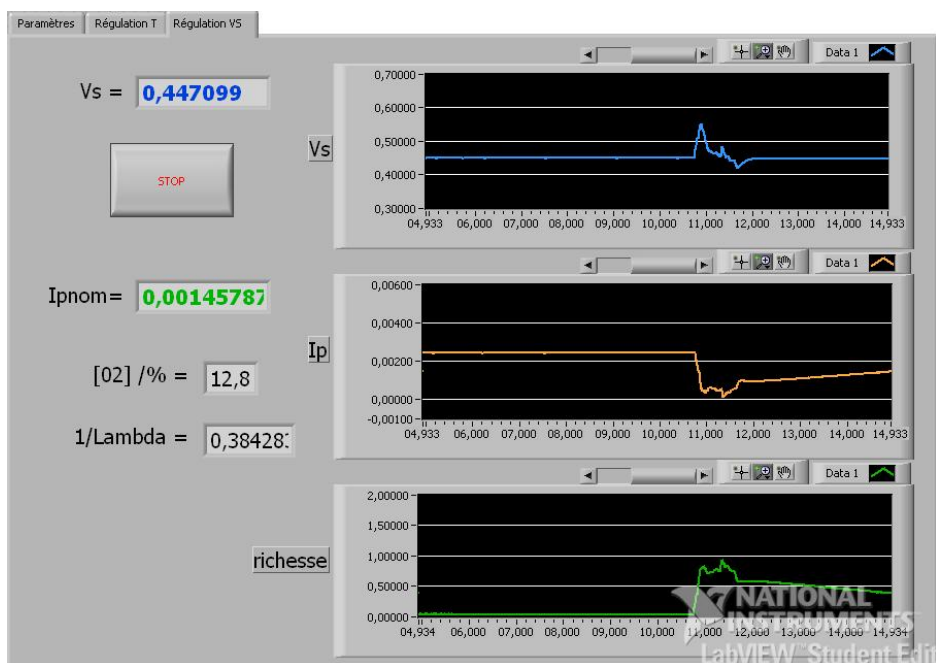
Figure D.2: Screenshot of the electrochemical signals acquisition tab.

Appendix E

Configuration of the TC1796 modules

<table>
<tr><th colspan="2"></th><th></th><th>Mode</th><th colspan="2">clock/match value</th><th>Output</th><th>action</th></tr>
<tr><td rowspan="16">GPTA</td><td rowspan="3">ADC requests</td><td>LTC0</td><td>Timer with reset</td><td>fgpta/2^7</td><td>586 kHz</td><td></td><td></td></tr>
<tr><td>LTC1</td><td>Compare with LTC0</td><td>0x0073</td><td>200 µs</td><td></td><td>set</td></tr>
<tr><td>LTC2</td><td>Compare with LTC0</td><td>0x0000</td><td></td><td>GPTA0_OUT3</td><td>reset</td></tr>
<tr><td rowspan="4">Ri pulse</td><td>LTC3</td><td>Timer with reset</td><td>fgpta/2^7</td><td>586 kHz</td><td></td><td></td></tr>
<tr><td>LTC4</td><td>Compare with LTC3</td><td>0xE482</td><td>100 ms</td><td></td><td>hold</td></tr>
<tr><td>LTC5</td><td>Compare with LTC3</td><td>0x0003</td><td>10 µs</td><td></td><td>reset</td></tr>
<tr><td>LTC6</td><td>Compare with LTC3</td><td>0x0078</td><td>210 µs</td><td>PIN 2.9</td><td>set</td></tr>
<tr><td rowspan="3">Ip PWM</td><td>LTC8</td><td>Timer with reset</td><td>fgpta/2</td><td>37.5 MHz</td><td></td><td></td></tr>
<tr><td>LTC9</td><td>Compare with LTC8</td><td>0x0EA4</td><td>10 kHz</td><td></td><td>set</td></tr>
<tr><td>LTC10</td><td>Compare with LTC8</td><td>0x0000</td><td>software controlled</td><td>PIN 3.2</td><td>reset</td></tr>
<tr><td rowspan="3">Heater PWM</td><td>LTC13</td><td>Timer with reset</td><td>fgpta/2^7</td><td>586 kHz</td><td></td><td></td></tr>
<tr><td>LTC14</td><td>Compare with LTC13</td><td>0x16E4</td><td>100 Hz</td><td></td><td>set</td></tr>
<tr><td>LTC15</td><td>Compare with LTC13</td><td>0x0000</td><td>software controlled</td><td>PIN 3.0</td><td>reset</td></tr>
<tr><td>Heat-up</td><td>LTC24</td><td>Free running Timer</td><td>fgpta/2^14</td><td>4.58 kHz</td><td></td><td>hold</td></tr>
</table>

<table>
<tr><th></th><th></th><th>Channel</th><th>Result register</th><th>Trigger source</th><th>Conversion time</th><th>Ref. voltage</th><th>Resolution</th></tr>
<tr><td rowspan="2">ADC</td><td>ADC0</td><td>2</td><td>0xF010073C</td><td rowspan="2">GPTA0_OUT3</td><td rowspan="2">1.52µs</td><td rowspan="2">3.3V</td><td rowspan="2">10bit</td></tr>
<tr><td>ADC1</td><td>3</td><td>0xF0100538</td></tr>
</table>

<table>
<tr><th></th><th></th><th>Channel</th><th>Source address</th><th>Trigger source</th><th>Destination</th><th># transfers</th><th>data width</th></tr>
<tr><td rowspan="2">DMA</td><td>Block 0</td><td>2</td><td>0xF010073C</td><td>ADC0</td><td>0xF010A080</td><td>5</td><td>16bit</td></tr>
<tr><td>Block 1</td><td>10</td><td>0xF0100538</td><td>ADC1</td><td>0xF010A000</td><td>5</td><td>16bit</td></tr>
</table>

Appendix F

Diagram of the control algorithms
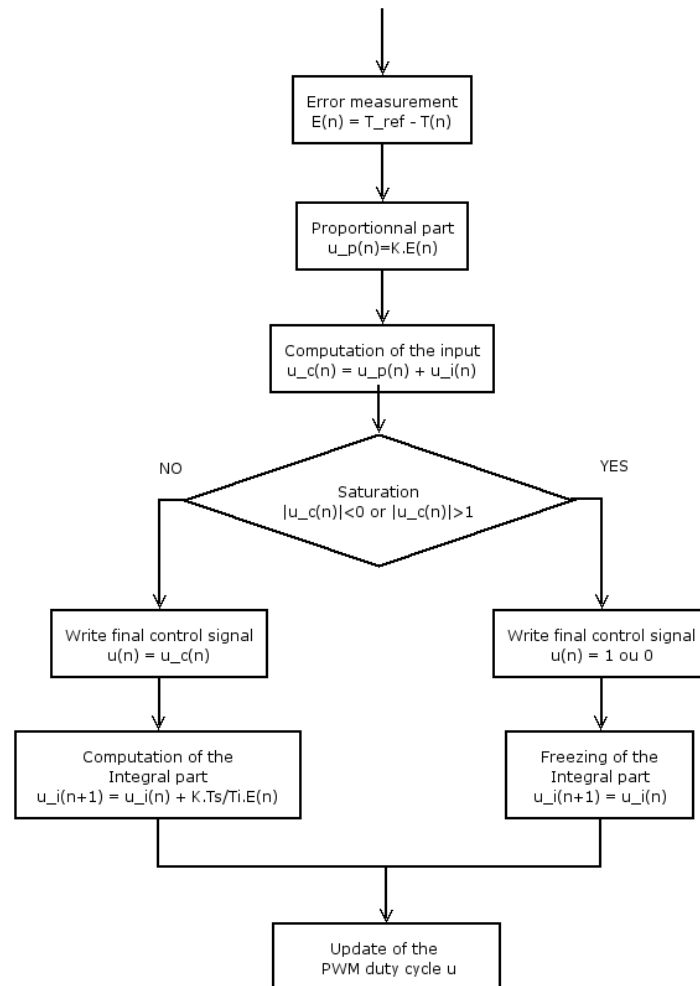
Figure F.1: Control procedures as they are implemented on the microcontroller.

Appendix G

Simulink model
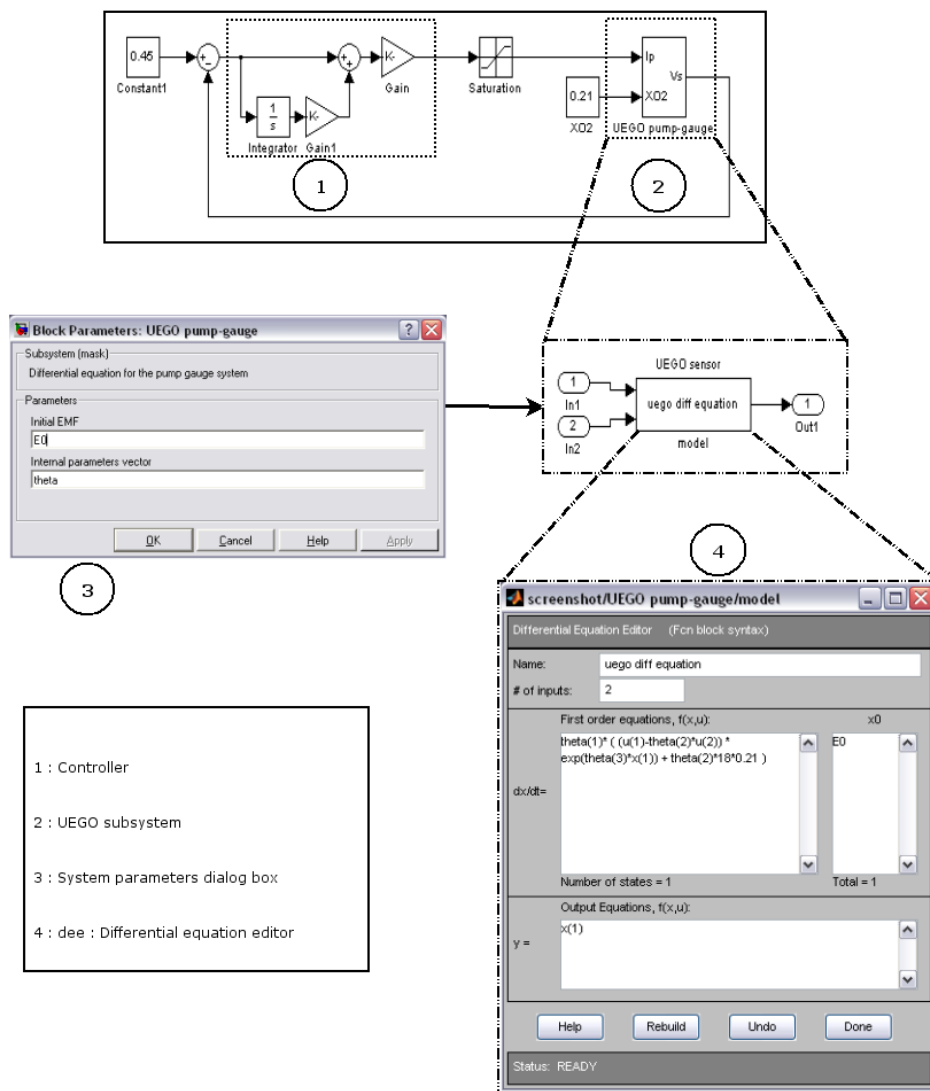
Figure G.1: Implementation of the sensor model using Simulink.

Appendix H

Gas bench results

Ce document présente brièvement les résultats des essais effectués sur banc gaz à Lardy le 28 Avril 2006 avec l'assistance de Mathieu Bourrat. Le but de ces analyses est de vérifier le bon comportement du système de contrôle de sondes proportionnelles basé sur microcontrôleur Tricore 1796 en présence de compositions gaseuses types.

H.1 Description du dispositif expérimental

Les figures H.1 et H.2 montrent le dispositif expérimental utilisé pour tester le système de contrôle par microcontrôleur. L'état de la sonde est donné par trois signaux extraits directement du microcontrôleur par liaison série avec un ordinateur équipé de LabVIEW. Ces trois signaux sont:

- la tension de Nernst V_s asservie à 0.45V

- le courant de pompage nominal $I_{p_{nom}}$ mesuré à travers une résistance de mesure de 61.9 Ω.

- la température interne de l'élément sensible T régulée autour de 780 °C

Les signaux V_s et $I_{p_{nom}}$ sont échantillonnés par le microcontrôleur à une fréquence de 200Hz alors que la température T est asservie à une fréquence de 10Hz. La valeur de la richesse[1] du milieu gazeux est calculée à partir du courant de pompage selon la charactéristique fournie par BOSCH[2].

La pression des gaz lors des essais était de 1013 hPa et leur température avoisinait les 450 °C.

---

[1]La richesse notée r est définie comme étant l'inverse du rapport air-carburant normalisé λ

[2]la loi de conversion, $\frac{0.0839 I_{p_{nom}}[\text{mA}]+1}{1-0.3901 I_{p_{nom}}[\text{mA}]}$, bien que valable en théorie uniquement pour des milieux pauvres ($r < 1$), a été utilisée dans les deux cas.
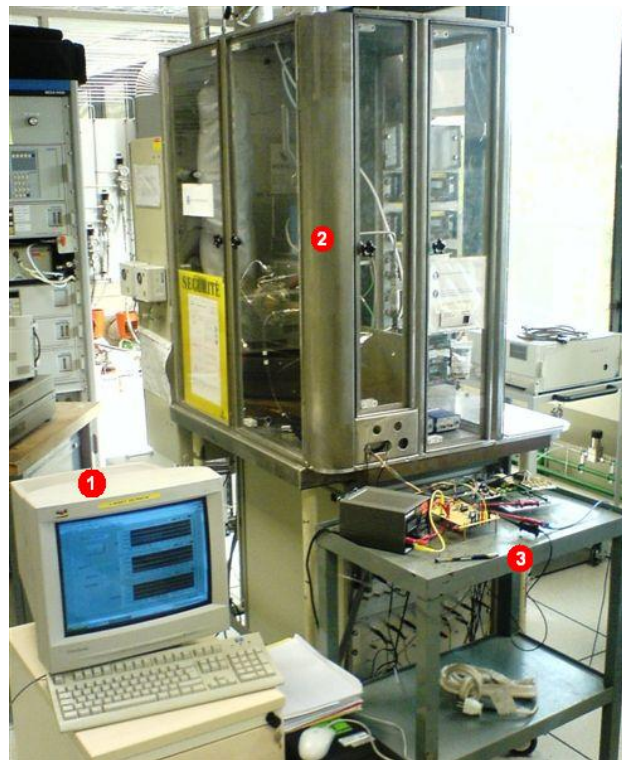
Figure H.1: Vue générale du dispositif expérimental (1: enregistrement des résultats par NI LabVIEW; 2: Banc gaz pour sondes proportionnelles; 3: microcontrôleur et interface électronique.
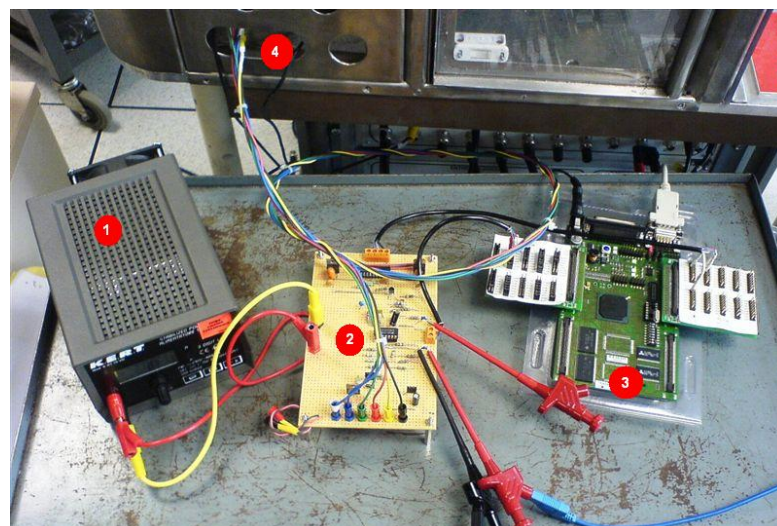

Figure H.2: Système de contrôle de la sonde proportionnelle (1: Alimentation 12V; 2: Circuit électronique d'interface; 3: Demoboard Tricore 1796; 4: vers sonde UEGO)

H.2   Analyse dynamique - Sauts de richesses

Afin d'évaluer les temps de réponse de la sonde et de son système de contrôle, le dispositif est soumis à des variations quasi instantanées de richesse. Les amplitudes de ces sauts de richesse sont celles couramment utilisées pour les sondes proportionnelles, à savoir des variations en milieu pauvre de 0.3 à 0.4 et en milieu riche de 0.5 à 1.05.

H.2.1   Saut de richesse 0.3-0.4

Les réponses des différentes variables du système sont données aux figures H.3 et H.4 et conduisent aux remarques suivantes:

- la température reste constante au cours de l'expérience

- la richesse indiquée par le microcontrôleur présente une erreur de 0.01 qui peut être liée au fait que les compositions gazeuses ne sont pas étalonnées. Il peut s'agir aussi d'un offset de l'électronique du système.

- la tension de Nernst s'écarte de moins de 15mV par rapport à la consigne de 450mV

- le temps de réponse de 10 à 90% en richesse est mesuré en considérant le courant de pompage[3]. Il est estimé à 70ms environ contre 145ms sur la même sonde contrôlée par boîtier AWS[4].
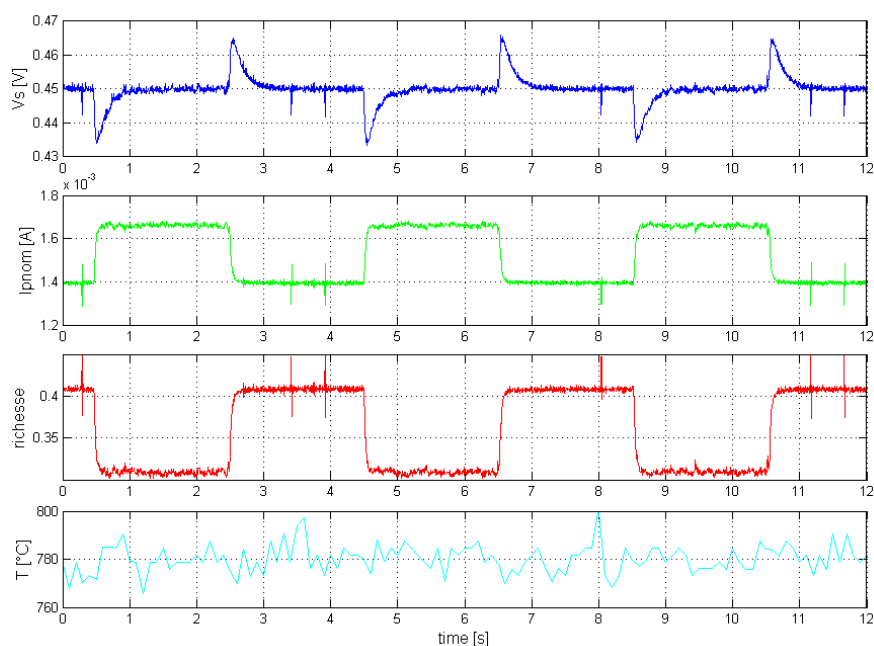

Figure H.3: Réponses dynamiques à des sauts de richesse de fréquence 0.25Hz.

---

[3]à ne pas confondre avec le temps de réponse du système régulé donné par l'allure de V_s
[4]système de contrôle BOSCH couramment utilisé sur banc gaz pour tester les sondes
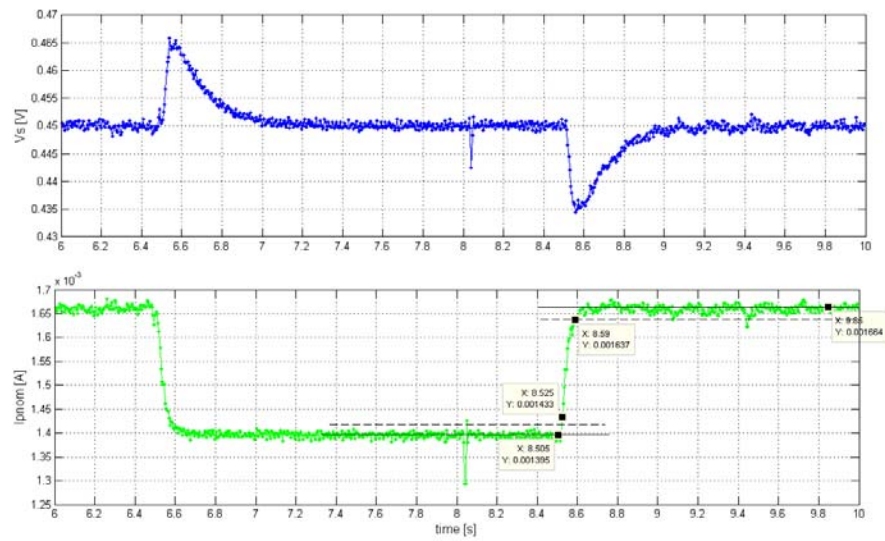
Figure H.4: Agrandissement des réponses temporelles sur un saut de richesse.

H.2.2   Saut de richesse 0.5-1.05

Les réponses des différentes variables du système sont données aux figures H.5 et H.6 et conduisent aux remarques suivantes:

- la température reste constante au cours de l'expérience

- la richesse indiquée par le microcontrôleur est conforme aux valeurs prévues. Le signal présente toutefois un léger affaissement qui pourrait provenir de la dissymétrie des électrovannes selon Mathieu Bourrat.

- la tension de Nernst s'écarte de 70mV par rapport à la consigne de 450mV

- le temps de réponse de 10 à 90% en richesse[5] est estimé à 50ms environ contre 138ms sur la même sonde contrôlée par boîtier AWS.

[5]en excluant le problème d'affaissement du signal
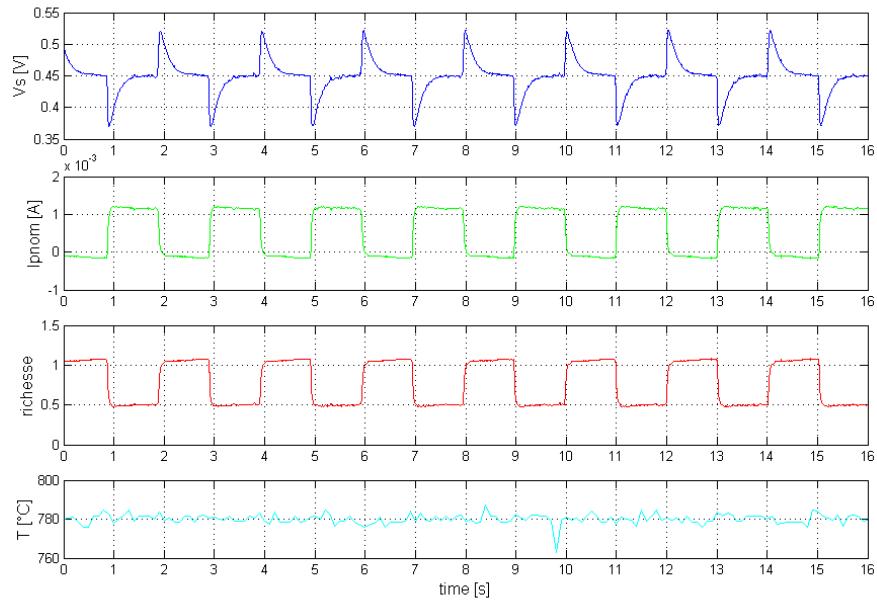
Figure H.5: Réponses dynamiques à des sauts de richesse de fréquence 0.5Hz
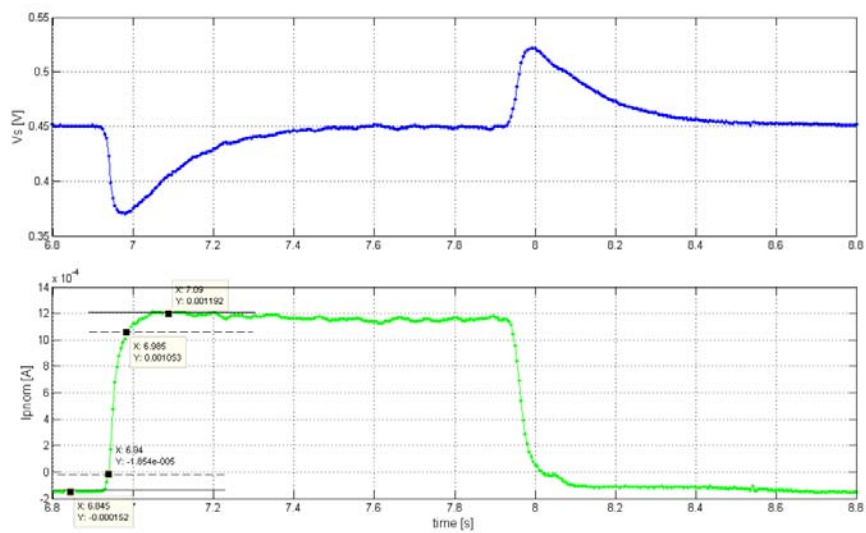
Figure H.6: Agrandissement des réponses temporelles sur un saut de richesse.

H.3 Analyse statique

Le tableau H.1 résume les résultats obtenus en régime permanent pour des compositions gaseuses riche et pauvre. La baie d'analyse HORIBA n'étant pas utilisée, les compositions sont fixées à priori. Dans chaque cas, la moyenne et l'écart type du courant de pompage et de la richesse sont calculés à partir des échantillons collectés. Un courant négatif est bien constaté en milieu riche, démontrant que la sonde et son système de contrôle réagissent aux gaz réducteurs issus d'une combustion en milieu riche. Ce point n'avait pas pu être vérifié auparavant.

| | | Ip | | r | |
		moyenne	σ	moyenne	σ
$T = 780°C$	*pauvre (0.1)*	2.066mA	3.9µA	0.1651	0.0013
	riche (1.05)	-0.3364mA	4.7µA	1.1641	0.0024
$T = 600°C$	*pauvre (0.1)*	1.893mA	6.2µA	0.2254	0.0022
	riche (1.05)	-0.1871mA	6.7µA	1.0901	0.0033

Table H.1: Charactéristiques statiques de la sonde pour deux niveaux de richesse et de température.

D'autre part, une série de mesures ont été effectuées afin d'estimer l'influence de la température sur les mesures de richesse. En général, la conductivité de la zircone devient critique à partir de 600 °C. La consigne de régulation de la température a donc été portée à cette valeur pour observer les conséquences sur le comportement du système. Lorsque la température est asservie à 600 °C, on constate une erreur de 10% par rapport à la valeur constatée à 780 °C.

H.4 Conclusions

Ces essais qualitatifs effectués sur banc gaz ont permis de démontrer le bon fonctionnement général de l'asservissement par microcontrôleur. Le principal enjeu consistait à soumettre le système à des gaz réducteurs (type CO, HC) dont l'influence n'avait pas pu être simulée auparavant. Fort heureusement, le pilotage par microcontrôleur est apparu opérationnel aussi bien en milieu riche qu'en milieu pauvre.

Il faut toutefois rappeler que ces essais n'ont pas le caractère officiel des essais classiques effectués sur banc gaz puisque les compositions gazeuses nétaient pas étalonnées.

Bibliography

[1] M Benammar: Techniques for measurement of oxygen and air-to-fuel ratio using zirconia sensors. A review. Meas. Sci. Technol. 5 (1994) p757-767

[2] M Benammar and W C Maskell: A leakage-tolerant zirconia pump-gauge oxygen sensor. Meas. Sci. Technol. 5 (1994) p1566-1571

[3] W C Maskell: Inorganic solid state chemically sensitive devices: electrochemical oxygen gas sensors. J. Phys. E: Sci. Instrum. 20 (1987) p1156-1168

[4] T S Auckenthaler, C H Onder and H P Geering: Modelling of a Solid-Electrolyte Oxygen Sensor. SAE technical paper 2002-01-1293

[5] E Ivers-Tiffée, K H Hardtl, W Menersklou, J Riegel: Principles of solid state oxygen sensors for lean combustion gas control. Electrochimica Acta 47 (2001) p807-814

[6] R P Sallen and E L Key: A practical method of designing RC active filters IEE Trans CT2 (March 1965) p74-85

[7] Collectif Automatique Supélec: Automatique. Polycopié Supélec 11049, 2003.

[8] K H Johansson: Lecture notes in 2E1245 Hybrid and Embedded Control Systems. School of Electrical Engineering, Royal Institute of Technology, Sweden, 20042006.